https://doi.org/10.5194/egusphere-2026-5285
Preprint. Discussion started: 17 September 2026

Tropical circulation and associated precipitation responses under idealized global warming simulations

Andreas Karpasitis[1], Manabu Abe[2], Isaline Bossert[3], Friederike Fröb[4], Thomas Frölicher[5], Panos Hadjinicolaou[1], Colin Jones[6], Roland Séférian[3], Tomas Torsvik[4], Jeremy Walton[7], Klaus Wyser[8], Tokuta Yokohata[9], and George Zittis[1]

[1]Climate and Atmosphere Research Center (CARE-C), The Cyprus Institute, Nicosia, Cyprus
[2]Japan Agency for Marine-Earth Science and Technology (JAMSTEC), Yokohama, Japan
[3]Météo-France, CNRS, Univ. Toulouse, CNRM, Toulouse, France
[4]Geophysical Institute, University of Bergen and Bjerknes Centre for Climate Research, Bergen, Norway
[5]Climate and Environmental Physics & Oeschger Centre for Climate Change Research, University of Bern, Bern, Switzerland
[6]National Centre for Atmospheric Science, University of Leeds, Leeds, UK
[7]Met Office Hadley Centre for Climate Science and Services, Exeter, UK
[8]Swedish Meteorological Hydrological Institute (SMHI), Norrköping, Sweden
[9]National Institute for Environmental Studies (NIES), Tsukuba, Japan

Correspondence: Andreas Karpasitis (a.karpasitis@cyi.ac.cy)

Abstract. The Inter-Tropical Convergence Zone (ITCZ) is a major precipitation feature in the global equatorial regions and a crucial part of the tropical atmospheric circulation. Due to its effects on the Hadley circulation, changes in the position and characteristics of the ITCZ can have a cascading impact not only in tropical regions that receive abundant precipitation throughout the year but also in adjacent sub-tropical regions that receive less rainfall, mostly in certain seasons. Aiming for a better understanding of tropical and sub-tropical precipitation dynamics, here we study the changes in the ITCZ position and characteristics, including the edges and strength, across various longitudinal bands for 2 ^oC and 4 ^oC Global Warming Levels (GWLs) above the pre-industrial conditions. Our analysis is based on idealized simulations from the Tipping Points Inter-comparison Project (TIPMIP). Shifts in the characteristics of the ITCZ are contrasted with the changes in the tropical and sub-tropical precipitation from these idealized experiments. Additionally, the variations in the regional zonal mean of the pressure velocity, as well as the global zonal mean of the mass streamfunction and pressure velocity, are assessed for both GWLs and compared with the modifications in the ITCZ location and associated precipitation. Our results show that the global zonal mean ITCZ will contract with a higher global mean temperature, with a general displacement toward the winter hemisphere. In the various regions, the ITCZ response to increasing global temperatures generally varies, but overall, weaker updrafts are projected. The precipitation intensity of the ITCZ band becomes stronger, despite the weakening of the Hadley cell circulation and its ascending and descending branches, with decreased precipitation projected in the descending branch over the sub-tropics.

https://doi.org/10.5194/egusphere-2026-5285
Preprint. Discussion started: 17 September 2026

1 Introduction

The tropical general atmospheric circulation is fundamentally structured around the Intertropical Convergence Zone (ITCZ), which is a region near the equator characterized by intense and widespread upward motion of air masses (Waliser and Somerville, 1994). This ascent is driven by strong surface heating under persistently high solar insolation and, in combination with the high moisture content of the tropical atmosphere, results in deep convection and heavy precipitation. The rising air diverges in the upper troposphere and moves poleward before subsiding in the sub-tropics, forming the descending branch of the Hadley circulation. Near the surface, this flow returns equatorward as the trade winds, closing the circulation (Stachnik and Schumacher, 2011). Branching off from the ITCZ are several persistent, semi-permanent areas of convergence located primarily over oceanic regions of the Southern Hemisphere. While distinct from the main ITCZ, features such as the South Pacific Convergence Zone (Vincent, 1994; Brown et al., 2020) and the South Atlantic Convergence Zone (Villela, 2017) act as prominent poleward extensions of this system.

Several methodologies have been proposed for identifying the ITCZ position (Nicholson, 2018; Byrne et al., 2018). Some of these approaches are based on the mass streamfunction (Byrne and Schneider, 2016b), while others rely on the pressure velocity (Zhou et al., 2020) or the energy flux (Bischoff and Schneider, 2014). Precipitation is another parameter that is regularly used to identify the ITCZ, due to the pronounced rainfall amounts that accompany it. For example, the precipitation centroid (Frierson and Hwang, 2012; Donohoe et al., 2013; Roldán-Gómez et al., 2022; Mischell and Lee, 2022) and the precipitation maximum (Liu et al., 2020; Ramotubei et al., 2025) have been proposed to identify the location of the ITCZ. Other methodologies are based on satellite observations, including the maximum cloudiness (Waliser and Gautier, 1993), or the Outgoing Long-Wave Radiation (Chopra et al., 2024). More complex definitions use multiple variables, such as wind divergence, along with wet bulb temperature (Berry and Reeder, 2014; Wodzicki and Rapp, 2016).

The position of the ITCZ in different parts of the planet is associated with many factors, such as the warming and cooling of the large ocean basins on multidecadal scales (Green et al., 2017), the inter-hemispheric sea surface temperature (SST) contrast (Mischell and Lee, 2022; Rajendran et al., 2013), the atmospheric energy flux (Adam et al., 2016a, b; Wei and Bordoni, 2020), cross-equatorial energy transport in the oceans, and aerosol radiative forcing (Zhang et al., 2021). The width of the ITCZ is partly governed by the radiative influence of upper-tropospheric clouds on the lower troposphere (Dixit et al., 2018). In turn, the annually averaged ITCZ width determines the meridional extent of the Hadley cell, since a narrower ascending branch confines the outflowing air to higher zonal momentum, causing it to become baroclinically unstable at a lower latitude and thereby contracting the Hadley cell poleward extent (Watt-Meyer and Frierson, 2019). In addition, the El-Niño Southern Oscillation (ENSO) has been found to affect the position of the Hadley cell and subsequently of the ITCZ on an inter-annual basis (Yun et al., 2021; Roldán-Gómez et al., 2022; Li et al., 2023).

Climate models are often subject to large biases in the tropical regions, which in turn leads to incorrect representation of the climate in the other parts of the globe, through the general atmospheric circulation, which originates in the tropics. The CMIP6 models, as the previous generations of CMIP models, are plagued by the double ITCZ problem (Tian and Dong, 2020), which is manifested mostly in the Central and Eastern Pacific as the erroneous simulation of two parallel precipitation bands

https://doi.org/10.5194/egusphere-2026-5285
Preprint. Discussion started: 17 September 2026

on either side of the equator, instead of a single ITCZ located primarily north of the equator. They also generally overestimate precipitation for most of the tropical land regions (Li et al., 2022), with most of the heavy tropical rainfall in the CMIP6 models being the result of the large-scale component, instead of the convection parameterizations (Yang et al., 2021), due to the inadequate spatial resolution.

Despite the discrepancies in how different climate models represent the ITCZ and the associated tropical weather, a consistent picture of its variability is emerging from the analysis of long-term observational records. Such observations indicate that, although the zonal mean position of the ITCZ has not changed significantly, in some regions (e.g., near the Americas), it has a northward trend, while in others (e.g., the Western Pacific), it has a southward trend (Liu et al., 2020). On inter-annual timescales, the ITCZ position migrates north and south in response to El Niño and La Niña, respectively (Ramotubei et al., 2025). On much longer timescales, there are indications from proxy data that the ITCZ has generally shifted northward since the Last Glacial Maximum, but by less than 3 degrees of latitude due to energetic constraints (Yuan et al., 2023).

Overall, future climate projections indicate that the annual and zonal-averaged ITCZ is expected to become narrower in a warmer planet (Byrne and Schneider, 2016a, b; Byrne et al., 2018), suggesting that the seasonal ITCZ is likely to shift equatorward. Other studies that explicitly focus on the seasonal migration of the ITCZ have found that the ITCZ, defined by the mid-tropospheric pressure velocity, is expected to move equatorward, become wider, and weaken (Zhou et al., 2020). In addition, climate models project that as the global average temperature rises, the Hadley cell is projected to widen (Grise and Davis, 2020; Son et al., 2018), which is an expected outcome of the scaling theory by Held (Schneider, 2006; Frierson et al., 2007), due to the increase of the static stability of the sub-tropical atmosphere, which in turn causes a poleward shift for the baroclinic eddies. The widening of the seasonally averaged ITCZ acts to further widen the Hadley cell, since in theory, it prevents the eddies from reaching lower latitudes (Watt-Meyer and Frierson, 2019). The strength of the Hadley cell, and of its ascending and descending branches, is expected to weaken (Hu et al., 2018). This response to a warmer climate is attributed to the mismatch between the increase in water vapour, which scales with the Clausius-Clapeyron equation (Vecchi and Soden, 2007), and the precipitation, which scales with the radiative cooling increase (Held and Soden, 2006). The precipitation in the equatorial regions is generally expected to intensify due to increased water vapour in the atmosphere (Vecchi and Soden, 2007), despite the weakening of the Hadley cell and the convective updrafts of the ITCZ (Held and Soden, 2006).

Research based on scenario simulations, such as SSP-driven CMIP6 projections, has clarified the large-scale response of tropical circulation to warming; however, the time-dependent nature of such forcing complicates the isolation of equilibrium responses at specific warming levels. In addition, regional changes in ITCZ structure remain insufficiently constrained. Idealized stabilization experiments provide a way to overcome both limitations. Accordingly, this study has three objectives: to quantify equilibrium changes in the ITCZ and Hadley cell at specified global warming levels; to assess the associated regional precipitation changes and circulation adjustments across the tropics and subtropics; and to develop an ITCZ identification methodology that complements existing approaches while improving its robustness and applicability for global-scale analyses.

https://doi.org/10.5194/egusphere-2026-5285
Preprint. Discussion started: 17 September 2026

2 Data

2.1 Earth System Models and idealized simulations

The Tipping Points Modelling Intercomparison Project (TIPMIP) project is an international collaboration that aspires to comprehensively broaden our perspective of tipping dynamics in various Earth system components and their uncertainties, using coupled ESMs (Winkelmann et al., 2025). It aims to assess the risk of crossing individual tipping points within the Earth system and to identify the processes and feedback mechanisms that drive these critical transitions.

The models participating in TIPMIP are forced with prescribed CO_2 emissions to achieve specific, predefined warming regimes. There are three main types of simulations: the ramp-up simulations, where the average temperature of the planet increases at a specific rate; the stabilisation runs, where the temperature of the planet is kept constant at specific Global Warming Levels by zeroing the CO_2 emissions; and the ramp-down runs, where the temperature decreases at a specific, predefined rate utilizing negative CO_2 emissions.

For both the pre-industrial control and stabilization experiments, a 50-year analysis period was selected. To ensure that the stabilization runs approached equilibrium, particularly with respect to ocean adjustment, the first 100 years of each simulation were excluded. The subsequent 50 years were then used for all analyses.

In this study, we focused on TIPMIP idealised simulations that follow the TIPMIP-ESM Tier 1 protocol (Jones et al., 2026). Specifically, zero-emission simulations that were initialized from the ramp-up simulation at the 2 ^oC and 4 ^oC GWL above the pre-industrial control runs are used. These are hereafter referred to as the 2 ^oC and 4 ^oC GWL stabilization simulations. These GWL stabilization runs are compared to the corresponding pre-industrial control runs (piControl). The models used are the EC-Earth3-ESM-1 (Döscher et al., 2022), UKESM1-2-LL (Sellar et al., 2019; Smith et al., 2021; Mulcahy et al., 2023), CRNM-ESM2-2 (Bossert et al., 2025), and IPSL-CM6-ESMCO2 (Boucher et al., 2020), GFDL-ESM2M (Dunne et al., 2012), MIROC-ES2L (Hajima et al., 2020) and NorESM2-LM (Øyvind Seland et al., 2020). The characteristics of each ESM, as well as the specific variants used in this study, are summarised in Table 1.

The different models use different Experiment IDs to indicate specific GWLs. For X.Y degrees of GWL, most models use the Experiment ID of esm-up2p0-gwlXpY (e.g., for 4.0 degrees of GWL, the stabilization run is denoted as esm-up2p0-gwl4p0). The exceptions are the NorESM2-LM, which uses the esm-up2p0-swlXpY, and the CNRM-CERFACS-ESM2-1, which uses the 02Kpd-XY naming scheme.

2.2 Reanalysis and observations

To verify the robustness of the ITCZ identification methodology described in Sect. 3.1, a brief evaluation was conducted using the different reanalysis and observational products. (see Appendix A). Specifically, the ERA5 reanalysis (Hersbach et al., 2020), the NCEP Reanalysis 2 (Kanamitsu et al., 2002), and the Global Precipitation Climatology Project (GPCP) gridded observations (Adler et al., 2018) were used. This evaluation was designed to confirm that the methodology yields physically realistic estimates of both the ITCZ core latitude and its latitudinal boundaries across the regions and seasons considered, thereby providing confidence in its applicability to real-world data.

https://doi.org/10.5194/egusphere-2026-5285
Preprint. Discussion started: 17 September 2026

Table 1. TIPMIP models that have been used in this study

Model name	Contributing Project	Atmospheric Resolution (km)	Oceanic Resolution (km)	Experiments / Ensemble members used
EC-Earth3-ESM-1	OptimESM	80	100	**esm-piControl**: r1i1p1f1 **esm-up2p0-gwl2p0**: r1i1p1f1, r3i1p1f1, r4i1p1f1, r5i1p1f1 **esm-up2p0-gwl4p0**: r1i1p1f1, r3i1p1f1, r4i1p1f1
UKESM1-2-LL	OptimESM	130	100	**esm-piControl**: r1i1p1f1 **esm-up2p0-gwl2p0**: r1i1p1f1 **esm-up2p0-gwl4p0**: r1i1p1f1
CNRM-ESM2-2	OptimESM	100	100	**esm-piControl**: r1i1p2f2 **02Kpd-20**: r1i1p2f2 **02Kpd-40**: r1i1p2f2
IPSL-CM6-ESMCO2	OptimESM	130	100	**esm-piControl**: r1i1p3f1 **esm-up2p0-gwl2p0**: r1i1p3f1 **esm-up2p0-gwl4p0**: r1i1p3f1
GDFL-ESM2M	TipESM	250	100	**esm-piControl**: r1i1p1f1 **esm-up2p0-gwl2p0**: r1i1p1f1 **esm-up2p0-gwl4p0**: r1i1p1f1
MIROC-ES2L	TipESM	500	100	**esm-piControl**: r1i1p1f1 **esm-up2p0-gwl2p0**: r1i1p1f1 **esm-up2p0-gwl4p0**: r1i1p1f1
NorESM2-LM	TipESM	250	100	**esm-piControl**: r1i1p1f1 **esm-up2p0-swl2p0**: r1i1p1f1 **esm-up2p0-swl4p0**: r1i1p1f1

2.3 Data processing

The ITCZ characteristics were computed by applying the algorithm to the seasonal mean of each year at the native model resolution. The analysis was conducted separately for each variant of each model. Multi-model means were constructed with equal model weighting; for models with multiple variants, an ensemble mean across variants was first calculated for each experiment and then included in the multi-model mean.

For the general circulation variables, all simulations were first regridded to a common $1^\circ \times 1^\circ$ grid using linear interpolation. Seasonal means were then calculated for each model across all available years and variants. Finally, the multi-model ensemble mean was derived from these model averages.

In the seasonal averaging, the December-January-February (DJF) season was defined using consecutive months, such that December from the previous calendar year was combined with January and February of each year.

https://doi.org/10.5194/egusphere-2026-5285
Preprint. Discussion started: 17 September 2026

3 Methodology

3.1 Definition of ITCZ characteristics

To identify the ITCZ location, we propose a methodology based on the precipitation centroid method, with modifications designed to improve robustness with respect to the chosen latitude bounds and to reduce the influence of extra-tropical precipitation, while still performing well over a limited zonal band. Instead of computing the centroid of precipitation over a fixed tropical latitude range, we first calculate zonal-mean precipitation and identify latitude intervals where precipitation exceeds a relative threshold defined as a fraction of the local maximum and the dominant precipitation band is selected. For this dominant band, a precipitation strength metric that accounts for both total precipitation and proximity to the equator is defined. The ITCZ latitude is finally defined as the precipitation-area-weighted centroid computed within the selected band only. This approach preserves the physical interpretation of the precipitation centroid while reducing sensitivity to latitude-range choices, enabling ITCZ identification in limited zonal regions, and minimising the influence of storm tracks, topography and other secondary precipitation features.

Specifically, to identify the ITCZ location in a zonal region with longitudes $\lambda \in [\lambda_1, \lambda_2]$ and within a latitude search domain $\phi \in [\phi_1, \phi_2]$ (which may either correspond to prescribed bounds or the full available latitude range), the zonal mean of precipitation $P(\phi, \lambda)$ between these longitudes is firstly calculated as follow using the original model resolution:

$$\bar{P}(\phi) = \frac{\int_{\lambda_1}^{\lambda_2} P(\phi,\lambda)d\lambda}{\int_{\lambda_1}^{\lambda_2} d\lambda}, \quad \phi \in [\phi_1, \phi_2] \tag{1}$$

The zonal-mean precipitation is then linearly interpolated onto a 0.1^o latitude grid, and a threshold is defined as follows:

$$P_{thr} = \alpha \max \bar{P}(\phi), \quad \alpha = 0.5 \tag{2}$$

The contiguous latitude bands (R_k) where the zonal mean exceeds this threshold are identified as:

$$\bar{P}(\phi) \geq P_{thr} \tag{3}$$

The peak latitude-weighted precipitation is calculated for each band as:

$$P_k = \max_{\phi \in R_k} (\bar{P}(\phi)\cos(\phi)) \tag{4}$$

In cases where two or more precipitation bands have peak latitude-weighted precipitation values exceeding 80% of the maximum, the selection of the dominant band depends on their hemispheric distribution. If at least one such peak occurs in each hemisphere, the dominant precipitation band is defined as the one located in the Northern Hemisphere that lies closest to the equator. If multiple qualifying peaks exist but are confined to a single hemisphere, the dominant band is instead defined as the one whose peak is closest to the equator. In all other cases, where only a single peak exceeds the threshold, it is identified as the dominant precipitation band:

$$k^* = \arg\max_k P_k \tag{5}$$

https://doi.org/10.5194/egusphere-2026-5285
Preprint. Discussion started: 17 September 2026

where R_{k^*} is the dominant precipitation region.

The precipitation strength of the dominant precipitation band is calculated as:

$$S_{k^*} = \int\limits_{\phi \in R_{k*}} \bar{P}(\phi)\cos\phi d\phi \tag{6}$$

Finally, the centroid of precipitation is computed within this dominant precipitation band R_{k^*} as:

$$\phi_{itcz} = \frac{\int_{\phi \in R_{k^*}} \phi \bar{P}(\phi)\cos\phi d\phi}{\int_{\phi \in R_{k^*}} \bar{P}(\phi)\cos\phi d\phi} \tag{7}$$

The northern and southern edges of the ITCZ are defined as the latitude bounds of the dominant precipitation band R_{k^*}. As a consistency check, to ensure that this diagnostic provides a physically meaningful representation of the ITCZ location and edges, we evaluated it using reanalysis data by comparing the diagnosed ITCZ location with the precipitation maps. This evaluation is provided in Appendix A.

In this study, the world is divided into seven different non-overlapping zonal regions, in addition to the global zonal mean. The selected region (with the longitude range in parentheses) are: America (-90^o, -40^o), Atlantic Ocean (-40^o, -10^o), Africa (-10^o, 40^o), Indian Ocean (40^o, 120^o), Western Pacific (120^o, 170^o), Central Pacific (170^o, 230^o) and Eastern Pacific (230^o, 270^o). These regions of interest are geographically defined in Fig. A1 for visual purposes. For each region, the ITCZ location and characteristics were calculated for the December-February (DJF) and June-August (JJA) seasons of each year in the study period.

3.2 Mass Streamfunction and Pressure Velocity

For the identification of the location and characteristics of the main circulation cells, the mass streamfunction was calculated from the seasonally averaged global zonal mean of the meridional wind (Hartmann, 2015):

$$\Psi(\phi,\rho) = \frac{2\pi\alpha\cos(\phi)}{g}\int\limits_{0}^{p} v dp \tag{8}$$

where α is the Earth's radius, g is the gravitational acceleration, v is zonal mean of the meridional velocity, ϕ is the latitude and p is the pressure level.

In tandem with the mass streamfunction, the regional and global zonal mean of the pressure velocity was used to more clearly identify regions of ascending and descending air columns, which are associated with the ascending and descending branches of the Hadley cell.

For the calculation of the circulation metrics, the mean between 800 and 300 hPa was calculated for both the mass streamfunction ($\bar{\Psi}$) and the pressure velocity ($\bar{\omega}$). The strength of the Hadley cell was then calculated as the maximum absolute value of $\bar{\Psi}$ along the latitudes, while for the strength of the updrafts, the minimum value of $\bar{\omega}$ across the latitudes. The edges of the Hadley cell were defined as the latitudes where $\bar{\Psi}$ crosses zero. These metrics were calculated separately for each model, and the multi-model mean and standard deviation were subsequently computed.

https://doi.org/10.5194/egusphere-2026-5285
Preprint. Discussion started: 17 September 2026

3.3 Vertical moisture transport

The vertical moisture transport, using large-scale atmospheric flow and hydrostatic approximations, is defined as:

$$F_q = -\frac{q \cdot \omega}{g} \tag{9}$$

where q is the specific humidity, ω is the pressure velocity, and g is the acceleration of gravity. In the analysis, the monthly values of $q \cdot \omega$ were first calculated, and then the ensemble averaging was performed as in the rest of the variables.

3.4 Robustness metric

The Signal-to-noise ratio (SNR) (Hawkins and Sutton, 2012; Mahony and Cannon, 2018) was used to assess the robustness of the change in the variables of individual models. The SNR is defined as:

$$SNR = \frac{|\Delta\mu|}{\sigma_{piControl}} \tag{10}$$

where $\sigma_{piControl}$ is the monthly temporal standard deviation of the variable in the piControl run and $\Delta\mu$ represents the difference of the temporal mean for the variable between the ensemble mean of the GWL runs and the piControl runs for each model separately:

$$\Delta\mu = \frac{\sum_{r=1}^{N} \mu_{GWL}}{N} - \frac{\sum_{r=1}^{M} \mu_{piControl}}{M} \tag{11}$$

where μ is the temporal mean of each variant. N and M are the number of variants of the GWL and piControl runs for the model, respectively.

4 Results

4.1 Precipitation changes

As the mean global temperature rises, precipitation patterns are expected to change across the globe. Figure 1 reveals a robust signal of wetter tropical and, to a lesser extent, polar regions and generally drier sub-tropics, especially for the $4\,^oC$ GWL. For the DJF season, large increases in precipitation are expected at both GWLs over the whole tropical Pacific, up to or exceeding +1 and +2 mm/day for the $2\,^oC$ and $4\,^oC$ GWL, respectively. Precipitation increases of up to 1 mm/day are also expected in the equatorial part of the Indian Ocean, especially in the $4\,^oC$ GWL. At the same time, decreases are expected in the sub-tropical regions, especially in the Pacific and Atlantic sectors, as well as in the southern Indian Ocean. For the JJA season, significant increases in precipitation are predicted in the tropical regions of the Pacific, but also near the Indian subcontinent. On the contrary, a notable decrease in precipitation is expected in Central America, with a more pronounced response at the higher GWL. Overall, tropical precipitation increases are slightly larger between the $4\,^oC$ and $2\,^oC$ GWLs than between the $2\,^oC$ GWL and the pre-industrial conditions, except in the Indian Ocean during the boreal summer. However, the changes are less robust over the central and eastern Pacific (Fig. S1).

https://doi.org/10.5194/egusphere-2026-5285
Preprint. Discussion started: 17 September 2026

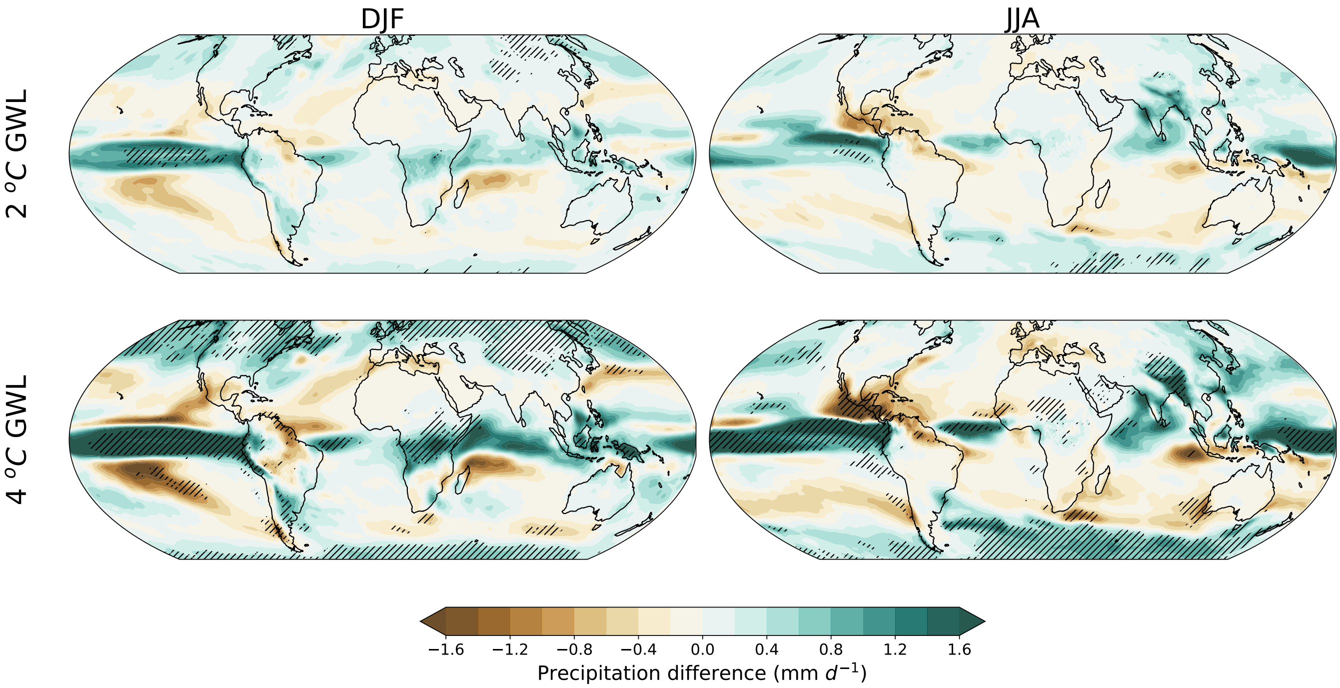

Figure 1. Multi-model mean precipitation differences between idealised stabilisation runs at 2 ^oC (top) and 4 ^oC (bottom) Global Warming Levels and Pre-Industrial control, for the December-to-February (DJF) season (left) and the June-to-August (JJA) season (right). Hatching denotes regions where at least 5 out of 7 models agree on the sign of change, and at least 4 out of 7 models show a robust signal-to-noise ratio (SNR>1).

4.2 Changes in ITCZ characteristics

Driven by changes in precipitation, the idealized experiments simulate several shifts in ITCZ location and width in response to global warming. For instance, in the American sector (Fig. 2), the models agree on a slight narrowing of the ITCZ in both seasons examined, most notably in JJA and under the highest GWL. At the same time, the ITCZ core shifts southward by less than 0.5° in JJA, whereas in DJF the models consistently indicate a small northward shift. In the Atlantic sector, the models project a southward displacement of both the northern ITCZ edge and the ITCZ core in JJA under the 4 ^oC GWL, while the southern edge shows no significant change. In DJF, however, there is no robust model agreement on changes in either the ITCZ location or its edges.

For the African sector, the ITCZ core and both edges shift northward in DJF, with the displacement exceeding 1 degree of latitude under the 4 ^oC GWL. For the JJA season, there is no significant change expected for the edges and the ITCZ location itself. Over the Indian Ocean, the ITCZ core and its southern edge are projected to shift northward in both seasons and under both GWLs, whereas no model agreement is found for the northern edge in either GWL, except in DJF under the 2 ^oC GWL, where a slight northward shift is indicated.

https://doi.org/10.5194/egusphere-2026-5285
Preprint. Discussion started: 17 September 2026

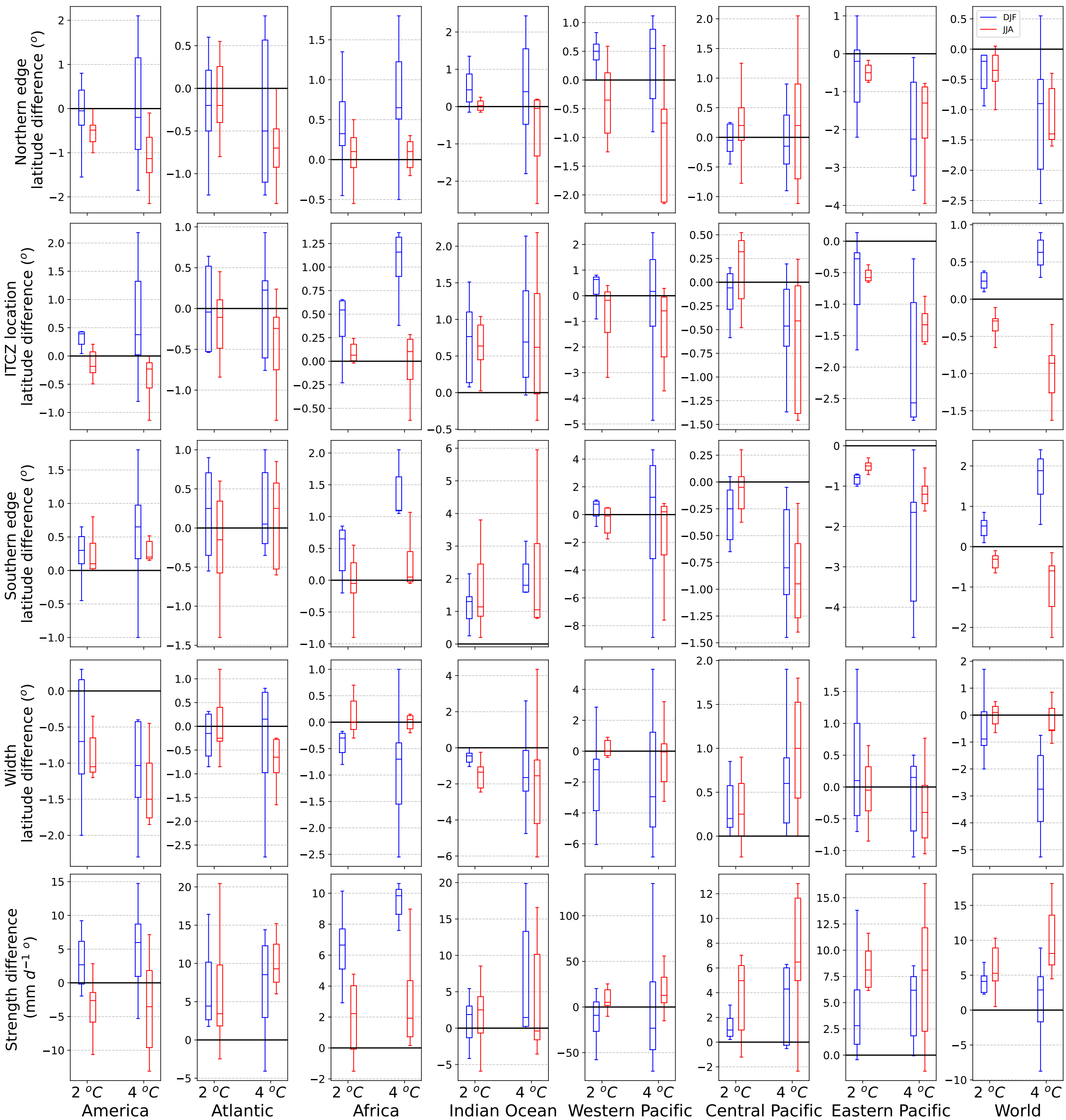

Figure 2. Boxplots of multi-model changes in the ITCZ characteristics (northern edge, ITCZ location, southern edge, width and strength) for 2 ^oC and 4 ^oC Global Warming Levels, compared to the pre-industrial control runs. The blue and red boxplots correspond to changes for the December to February (DJF) and June to August (JJA) seasons, respectively.

https://doi.org/10.5194/egusphere-2026-5285
Preprint. Discussion started: 17 September 2026

The Pacific basin also shows clear regional contrasts in the modeled ITCZ response. For the Western Pacific sector, the models indicate a slight southward displacement of the northern edge and the ITCZ core in JJA under the $4\ ^oC$ GWL, whereas in DJF under the $2\ ^oC$ GWL a small northward shift is projected. In the Central Pacific sector, no significant change is projected for the northern edge in either GWL or season; however, under the $4\ ^oC$ GWL, the ITCZ core and southern edge shift southward in both seasons. In the Eastern Pacific sector, all ITCZ characteristics shift southward in both seasons, with the signal becoming more pronounced at the higher GWL. Overall, the DJF changes are generally larger than those in JJA.

For the global zonal mean, the ITCZ core and its southern edge are projected to shift northward in DJF, whereas both move southward in JJA. The northern edge shifts southward in both seasons and at both GWLs, with the signal becoming more pronounced at the higher GWL.

Generally, as a response to the global and equatorial warming, the precipitation intensity of the ITCZ is expected to increase for both seasons and in most sectors, with some exceptions for the Americas, Indian Ocean, and Western Pacific. For the American sector, in particular, the strength of the ITCZ is expected to become slightly stronger in DJF and slightly weaker in JJA, especially in the $2\ ^oC$ GWL. In the Indian Ocean, many models indicate a strengthening in the $2\ ^oC$ GWL for both seasons, but there is no model consensus for the JJA season of the $4\ ^oC$ GWL. In the Western Pacific sector, a significant increase in the ITCZ intensity is projected mostly for the JJA season, but for the DJF season, there is no agreement between the models on the change in strength predicted.

Comparing these ITCZ changes (Fig.2) with the precipitation response (Fig.1) reveals broad agreement. In the American sector, the modest shifts in ITCZ location, edges, and intensity are consistent with the minimal precipitation changes over northern South America. In the African sector, the strengthening of the ITCZ in DJF aligns with pronounced precipitation increases over central Africa, whereas in JJA the weak ITCZ changes are reflected in only minor precipitation differences. Over the Indian Ocean, the precipitation dipole is consistent with the northward displacement of the ITCZ core and its southern edge in both seasons. In the Western Pacific, the marked precipitation increases, especially in JJA, are mirrored by a substantial intensification of the ITCZ during that season. In the Central and Eastern Pacific, the large projected precipitation increases in both seasons are generally accompanied by only modest increases in ITCZ intensity.

4.3 Pressure Velocity changes

Pressure velocity responses to global warming were also examined to assess changes in the ascending and descending branches of the Hadley cell (Figs. 3, 4, and S2). Across the different longitudinal sectors, the pressure velocity changes at the $2\ ^oC$ GWL (Fig. 3) generally have the same sign as those at the $4\ ^oC$ GWL (Fig. 4), although they are weaker in magnitude and less robust. Furthermore, the changes between $4\ ^oC$ and $2\ ^oC$ (Fig. S2) closely resemble those between the $2\ ^oC$ GWL and the piControl simulation. Consequently, Fig. 3 is not discussed further.

In the American sector, a $4\ ^oC$ warmer climate is associated with a weakening of both ascending and descending motions (Fig. 4). This response is particularly pronounced in the middle troposphere during both seasons considered, alongside a deeper vertical extension of the ascending and descending branches in the upper parts of the atmosphere, which leads to a higher tropical tropopause. In JJA, the decrease in intensity is focused in the northern part of the updrafts, which indicates

https://doi.org/10.5194/egusphere-2026-5285
Preprint. Discussion started: 17 September 2026

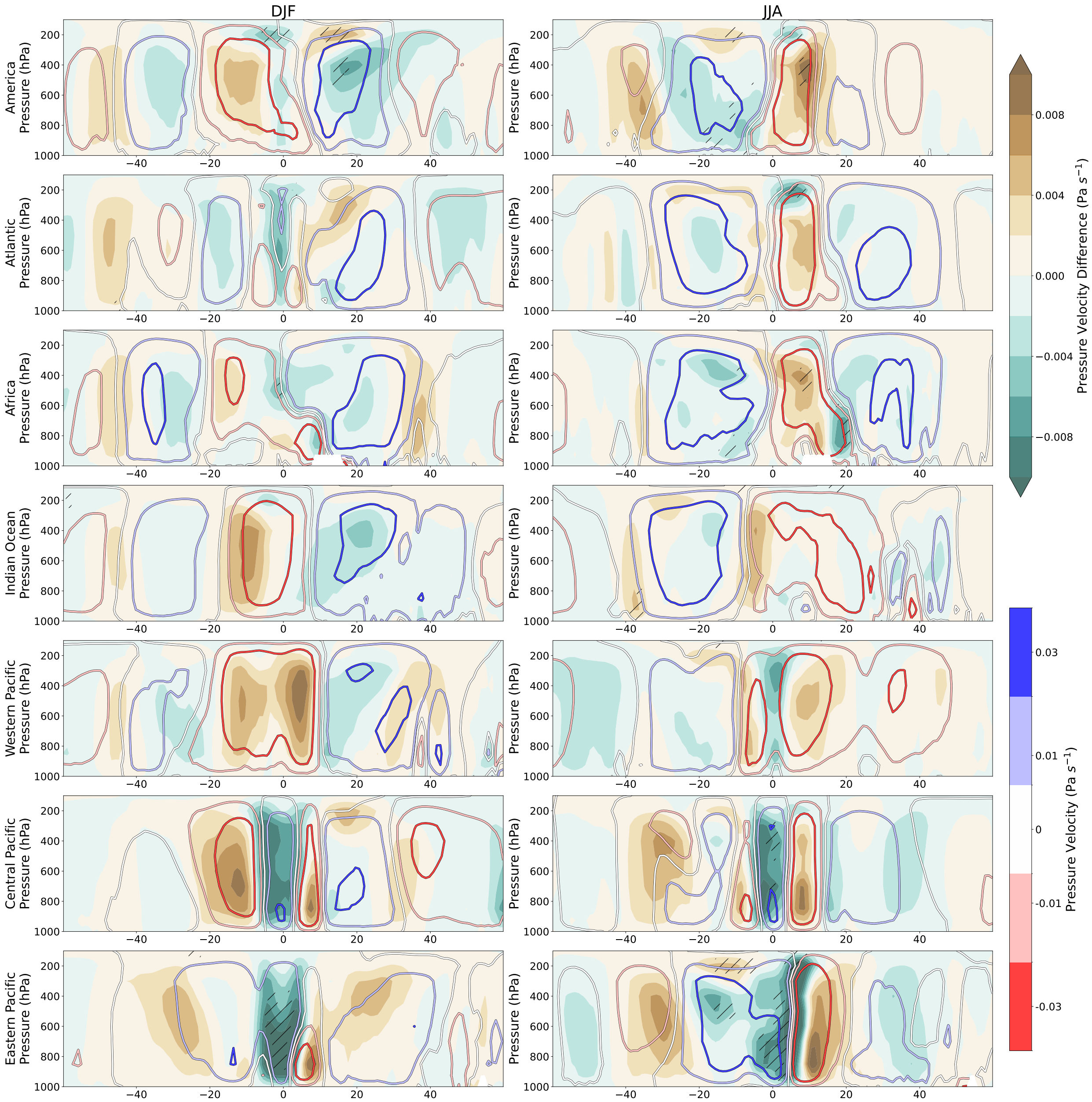

Figure 3. Zonal mean of multi-model mean pressure velocity changes between 2 ^oC GWL and piControl for the different longitudinal regions, for the DJF (left) and JJA (right) seasons. The multi-model mean of the change is shown with filled contours, while the solid contours indicate the values of the multi-model mean climatology for the piControl run. Hatching denotes regions where at least 5 out of 7 models agree on the sign of change and where at least 4 out of 7 models show a robust signal-to-noise ratio (SNR>1). Positive values of the pressure velocity mean downward velocities, and negative values mean upward velocities.

https://doi.org/10.5194/egusphere-2026-5285
Preprint. Discussion started: 17 September 2026

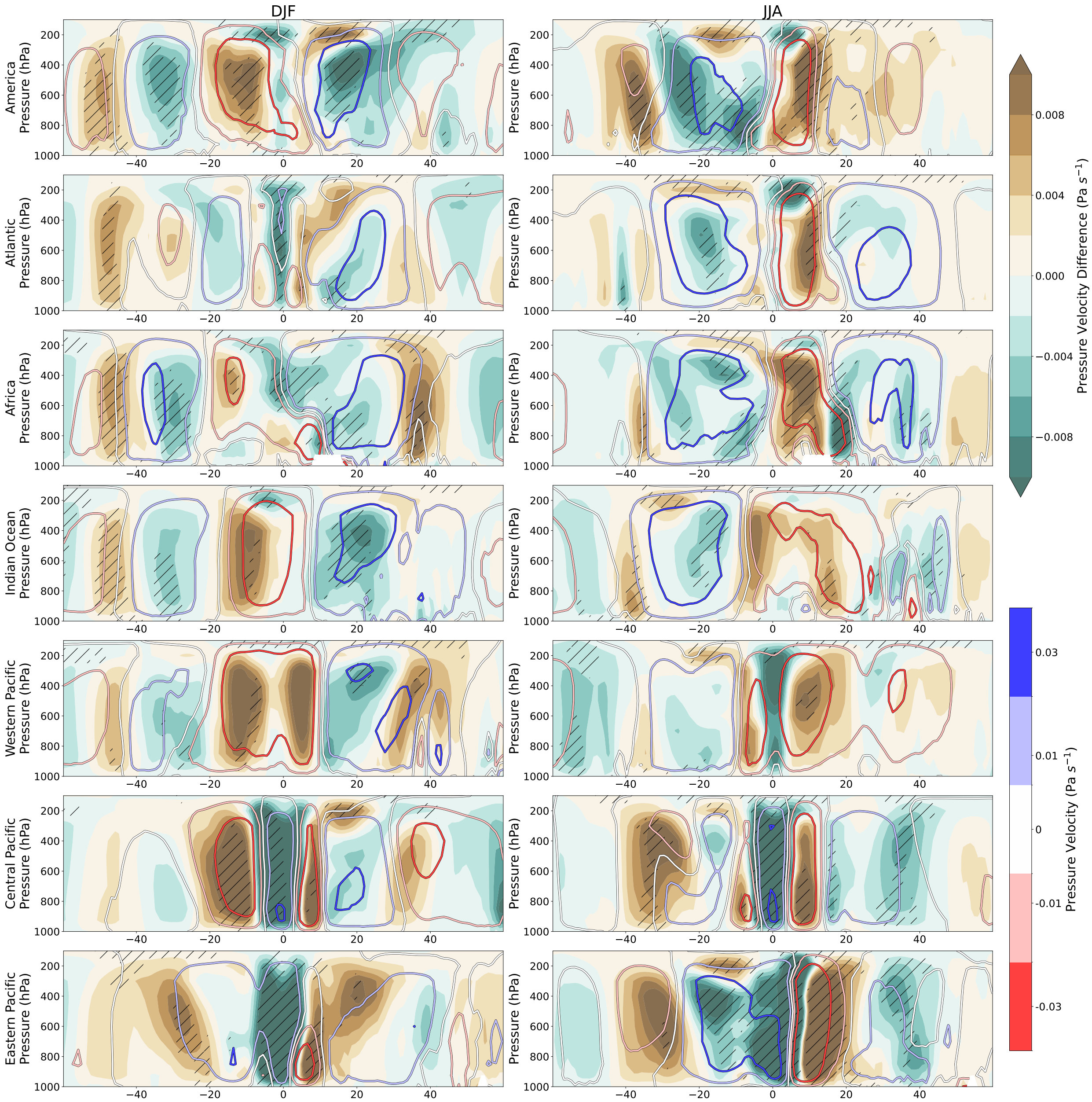

Figure 4. Same as Fig. 3 but for the 4 ^oC Global Warming Level

a southward shift of the northern edge of the updrafts, in agreement with Fig. 2. In the Atlantic sector, ascending motion is generally weak in DJF, but is projected to weaken further at the 4 ^oC GWL. In JJA, a similar weakening is projected in the northern portion of the ascending branch, accompanied by a deeper extension of ascent into the upper troposphere. Over Africa, substantial weakening of both ascending and descending motions is projected in JJA under global warming, together with a

https://doi.org/10.5194/egusphere-2026-5285
Preprint. Discussion started: 17 September 2026

northward extension of the ascending branch in the lower troposphere. In DJF, a more modest weakening of ascending and descending motions is projected. Over the Indian Ocean, ascending motion weakens primarily in the southern portion of the ascending branch in both seasons, while descending motion weakens in both hemispheres. This pattern is consistent with the northward displacement of the ITCZ and its southern edge shown in Fig. 2.

The Pacific sectors exhibit the largest responses compared with all other regions. In the western Pacific, a significant weakening of ascending motion is evident during boreal winter. During boreal summer, the dipole pattern of pressure-velocity changes indicates a southward displacement of the ascending branch.

In the central Pacific, ascending motion is simulated to weaken substantially in both hemispheres and during both seasons. This weakening is accompanied by a reduction in the intensity of descending motion over the equatorial region. In the Eastern Pacific during DJF, ascending motion associated with the southern branch of the ITCZ intensifies, whereas that associated with the northern branch weakens. Both ascending branches remain shallow, however, and do not extend beyond the middle troposphere. These changes are accompanied by a slight strengthening of the southern edges of the sub-tropical descending branch and a weakening of descending motion over the equatorial region. During JJA, a pronounced dipole in pressure-velocity changes extends throughout the troposphere, indicating a southward shift of the ascending branch, which is predominantly located in the Northern Hemisphere. This shift is accompanied by a substantial weakening of descending motion at and south of the Equator.

4.4 Global general circulation changes

Introducing the large-scale circulation response, Figure 5 and Table 2 show a robust weakening of the main Hadley cell in both seasons under the 2 °C GWL relative to piControl. In DJF, the Hadley cell intensity is projected to decrease by about 7%, while both the southern and northern edges are expected to shift slightly northward by approximately 0.7 and 0.4 degrees of latitude, respectively. In JJA, the Hadley cell strength is projected to decrease by 5%, with the southern edge shifting southward by 0.8 degrees and the northern edge moving northward by about 1 degree relative to piControl.

Examining the global zonal mean of pressure velocity, a slight weakening of both downdrafts and updrafts is generally projected along the descending and ascending branches of the Hadley cell in both seasons. During DJF, the ITCZ updrafts are not expected to change substantially in intensity, but they do shift northward, consistent with a northward displacement of the Hadley cell's southern edge and weaker downdrafts along its opposite edge. These circulation changes are accompanied by a precipitation dipole, with increased rainfall just south of the equator and reduced rainfall to the north. During JJA, a slight southward shift and weakening of the main updrafts by about 4% along the northern edge of the Hadley cell is expected in a 2 ^oC warmer world, with weakened downdrafts on the opposite end of the Hadley cell. The displacement of the ITCZ updrafts is associated with increased precipitation at these latitudes and reduced precipitation in the downdraft regions.

For the 4 ^oC GWL, similar changes to those shown in Fig. 5 are projected when compared to the 2 ^oC GWL (Fig. S3). Relative to the pre-industrial conditions, however, the 4 ^oC GWL exhibits more pronounced changes (Fig. 6; Table 2), with stronger model agreement across the zonal section. A pronounced weakening of the main Hadley cells by about 15% is observed for both seasons. For the DJF season, there is a slight northward displacement of both edges of the Hadley cell

https://doi.org/10.5194/egusphere-2026-5285
Preprint. Discussion started: 17 September 2026

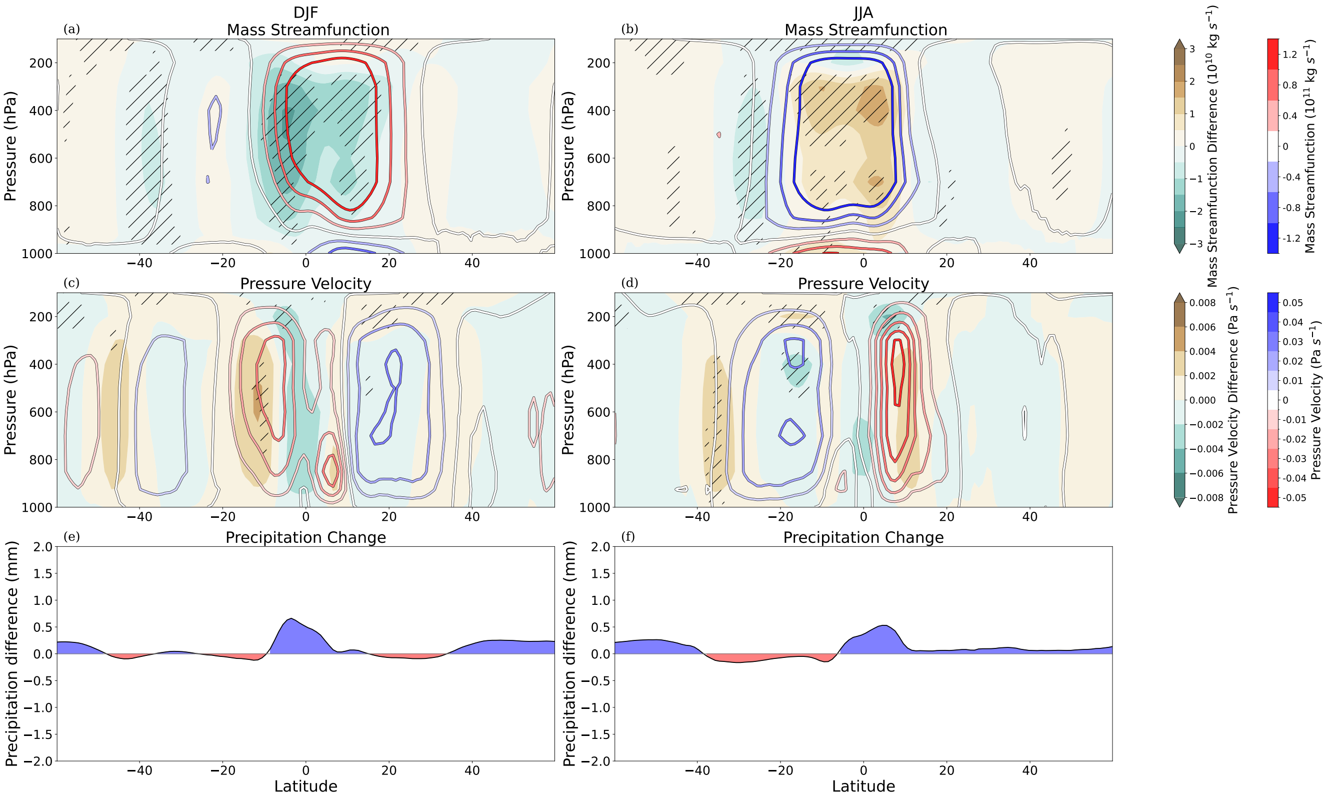

Figure 5. Multi-model mean circulation changes between 2 ^oC GWL and piControl. Zonal mean mass streamfunction changes are shown for the (a) DJF and (b) JJA seasons, with filled contours, while solid contours indicate the values of the multi-model mean climatology for the piControl run. Panels (c) and (d) are as in (a) and (b), but for the pressure velocity. Panels (e) and (f) show the changes in the zonal mean of precipitation between the stabilisation run and the piControl run for the DJF and JJA seasons, respectively. Hatching denotes regions where at least 5 out of 7 models agree on the sign of change and where at least 4 out of 7 models show a robust signal-to-noise ratio (SNR>1). Positive values of mass-streamfunction indicate clockwise direction of movement, and negative values indicate counter-clockwise direction.

by about 1 degree of latitude. In the summer season, both edges of the Hadley cell are expected to be displaced poleward in their respective hemispheres by about 2 degrees.

Table 2 shows no weakening of the main updrafts in DJF, while in JJA there will be large decrease in intensity approaching 11%, with a more pronounced northward (southward) displacement of the updrafts in the DJF (JJA) season. Additionally, there is a larger increase in precipitation at the location of the ITCZ updrafts for both seasons, compared to the piControl, with a decrease in precipitation in the descending regions on the opposite end of the Hadley cell.

An increase in the vertical moisture transport in the tropical regions, between 10^o S and 10^o N, during both seasons and GWLs, is expected, most notably in the lower and middle troposphere (Figure 7). In the sub-tropical regions of both hemispheres, a decrease in the vertical moisture transport is projected in all scenarios. In the winter hemisphere, this decrease in

https://doi.org/10.5194/egusphere-2026-5285
Preprint. Discussion started: 17 September 2026

Table 2. General circulation metrics for the multi-model mean

Season	Run	Hadley cell (HC) strength ($10^{11}\ kg\ s^{-1}$)	Southern edge of HC (^{o} latitude)	Northern edge of HC (^{o} latitude)	Updrafts strength ($10^{-2}\ Pa\ s^{-1}$)
DJF	piControl	1.92±0.15	-13.2±1.5	28.2±0.6	-3.36±0.54
	2 ^oC GWL	1.78±0.17	-12.5±1.3	28.6±0.6	-3.34±0.64
	4 ^oC GWL	1.62±0.14	-12.0±1.4	29.1±0.7	-3.37±0.61
JJA	piControl	2.06±0.21	-26.9±1.0	16.6±1.9	-5.21±0.27
	2 ^oC GWL	1.95±0.17	-27.7±0.9	17.6±1.9	-5.02±0.24
	4 ^oC GWL	1.75±0.14	-28.5±0.9	19.3±3.3	-4.66±0.43

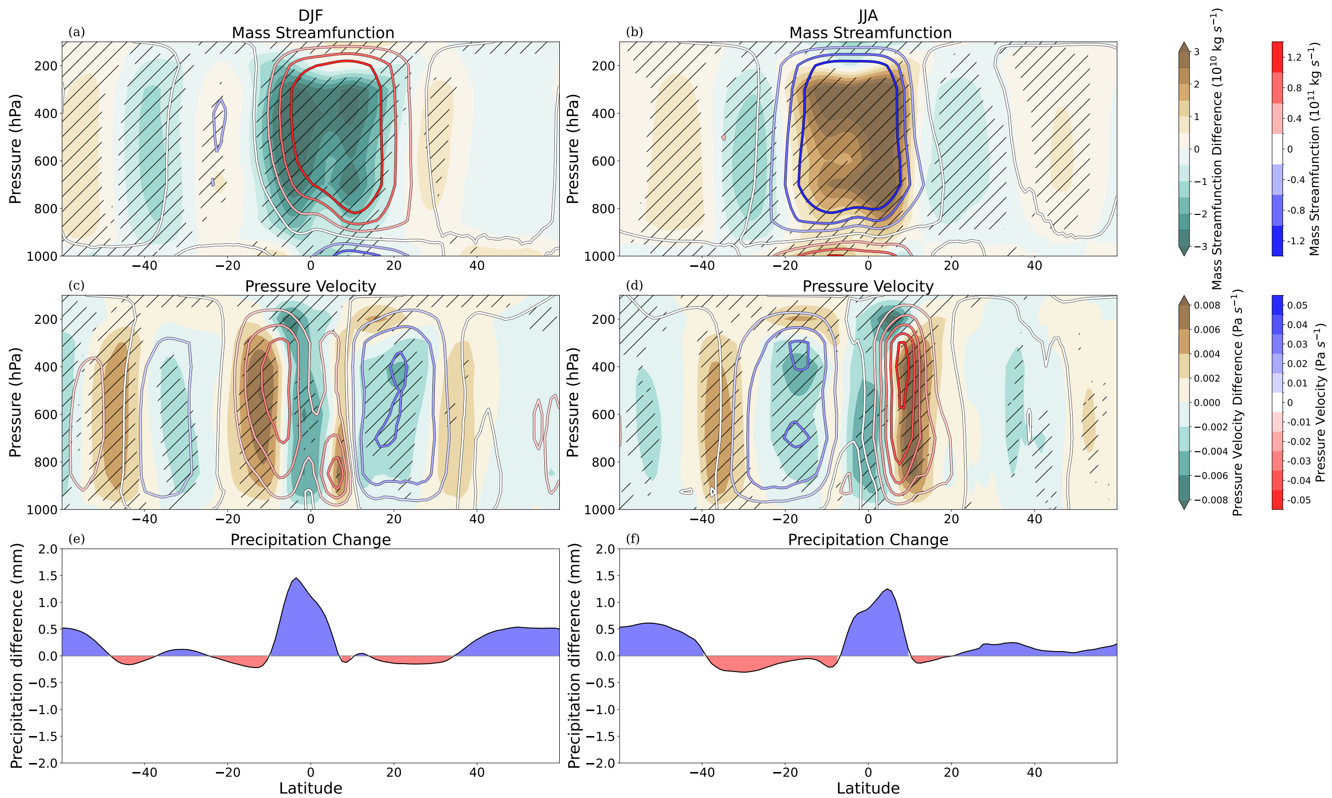

Figure 6. Same as Fig. 5 but for the 4 ^oC Global Warming Level.

vertical transport of moisture covers a wide band between 10^o and 40^o of the corresponding hemisphere, and extends throughout the troposphere. On the other hand, in the summer hemisphere, the decrease in the vertical moisture transport in the sub-tropics is confined in the latitude band between 10^o and 20^o of the corresponding hemisphere, and does not extend beyond the middle troposphere. In the 4 ^oC GWL, there is a more robust signal across the latitudes and pressure levels for the projected changes.

https://doi.org/10.5194/egusphere-2026-5285
Preprint. Discussion started: 17 September 2026

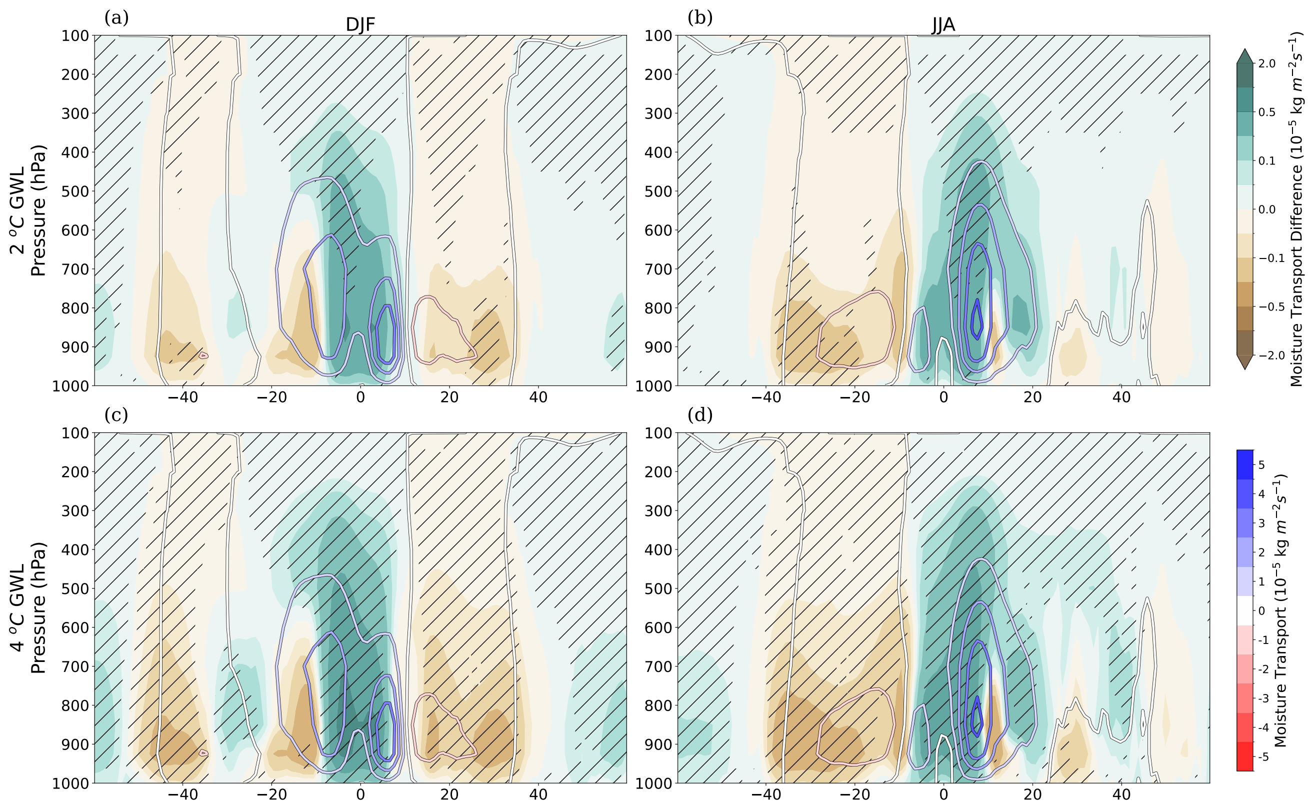

Figure 7. Multi-model mean vertical moisture transport changes between 2 ^oC and 4 ^oC GWLs and Pre-Industrial control. With filled contours, the changes are shown for DJF (left) and JJA (right) seasons, while solid contours indicate the values of the multi-model mean climatology for the piControl run. Hatching denotes regions where at least 5 out of 7 models agree on the sign of change and where at least 4 out of 7 models show a robust signal-to-noise ratio (SNR>1).

5 Conclusions

The Intertropical Convergence Zone (ITCZ) is a global precipitation feature that is highly sensitive to global warming. Changes in its location and intensity can therefore have substantial consequences for ecosystems and socio-economic activities across the tropics and beyond. Here, we propose an ITCZ identification methodology that complements existing approaches and demonstrates robust performance across most regions of the globe. For example, in the eastern Pacific, climate models often simulate a southern branch of the double ITCZ that is as strong as, or stronger than, its northern counterpart. In such cases, our detection algorithm adapts by identifying the ITCZ position between the two hemispheric branches.

Using idealised equilibrium simulations at predefined global warming levels (GWLs), we investigated changes in tropical precipitation, ITCZ characteristics, and Hadley cell structure. In the global zonal mean, the ITCZ narrows during boreal winter, while its northern edge shifts southward in both seasons. Overall, the ITCZ core tends to move towards the winter hemisphere,

https://doi.org/10.5194/egusphere-2026-5285
Preprint. Discussion started: 17 September 2026

with larger displacements at the higher GWL, and with its southern edge shifts following it. The apparent narrowing partly reflects the quantile-based definition used to diagnose the ITCZ edges.

At the regional scale, changes in ITCZ position generally correspond to projected precipitation changes shown in Fig. 1. For example, the northward displacement of the southern edge of the Indian Ocean ITCZ is consistent with the projected precipitation dipole in this region during both seasons. ITCZ precipitation intensity increases across most regions, with exceptions over the continental equatorial America and Africa in JJA. This widespread intensification is consistent with the projected increase in precipitation across much of the equatorial belt.

Regional ITCZ displacements generally become more pronounced at the higher GWL, although uncertainty also increases where the simulated changes are small. This is evident, for example, for the northern edge of the central Pacific ITCZ during both seasons.

The ascending and descending branches associated with the Hadley circulation weaken in most regions, with the largest responses occurring over the central and eastern Pacific. Although ascending motion weakens through much of the troposphere, some regions exhibit a slight strengthening in the upper troposphere, which leads to a higher tropopause.

The mass streamfunction analysis indicates a weakening of the Hadley circulation in both seasons, with a greater decrease in the higher GWL. This weakening of the Hadley cell agrees with Hu et al. (2018). The zonal mean of the pressure velocities shows that the ascending branch of the Hadley cell is being displaced towards the winter hemisphere, in agreement with the displacement of the ITCZ location. These plots also signify that the descending and ascending branches of the Hadley cell will become slightly weaker. This weakening of the Hadley cell in warmer climates is caused by the mismatch in the increase of water vapor in the tropical atmosphere, which scales with the Clausius-Clapeyron relation by about $7\%K^{-1}$ (Vecchi and Soden, 2007), and the increase in precipitation, which scales with the radiative cooling increase by about $2\%K^{-1}$ (Held and Soden, 2006; Vecchi and Soden, 2007). As a result, there is a reduction in the convective mass flux in the tropics (Held and Soden, 2006; Su et al., 2014; Kjellsson, 2015), in order to maintain the global water balance, which translates to weaker updrafts and weaker Hadley cell circulation.

Despite the weakening of ascending motion, precipitation associated with the ITCZ generally intensifies. Higher tropical temperatures increase atmospheric moisture availability and enhance vertical moisture transport over tropical regions (Fig. 7), thereby supporting increased precipitation. In contrast, the sub-tropical descending branches are generally associated with reduced precipitation and moisture fluxes.

The ITCZ and tropical-circulation changes identified here provide insight into processes that may contribute to non-linear responses of the tropical climate system at different GWLs. Because the ITCZ plays a central role in tropical precipitation and atmospheric energy transport, clarifying its response to warming is essential for identifying mechanisms that may amplify regional climate change. By examining equilibrium responses across warming levels and longitudinal sectors, this study advances understanding of tropical climate sensitivity and its implications for regional water availability.

https://doi.org/10.5194/egusphere-2026-5285
Preprint. Discussion started: 17 September 2026

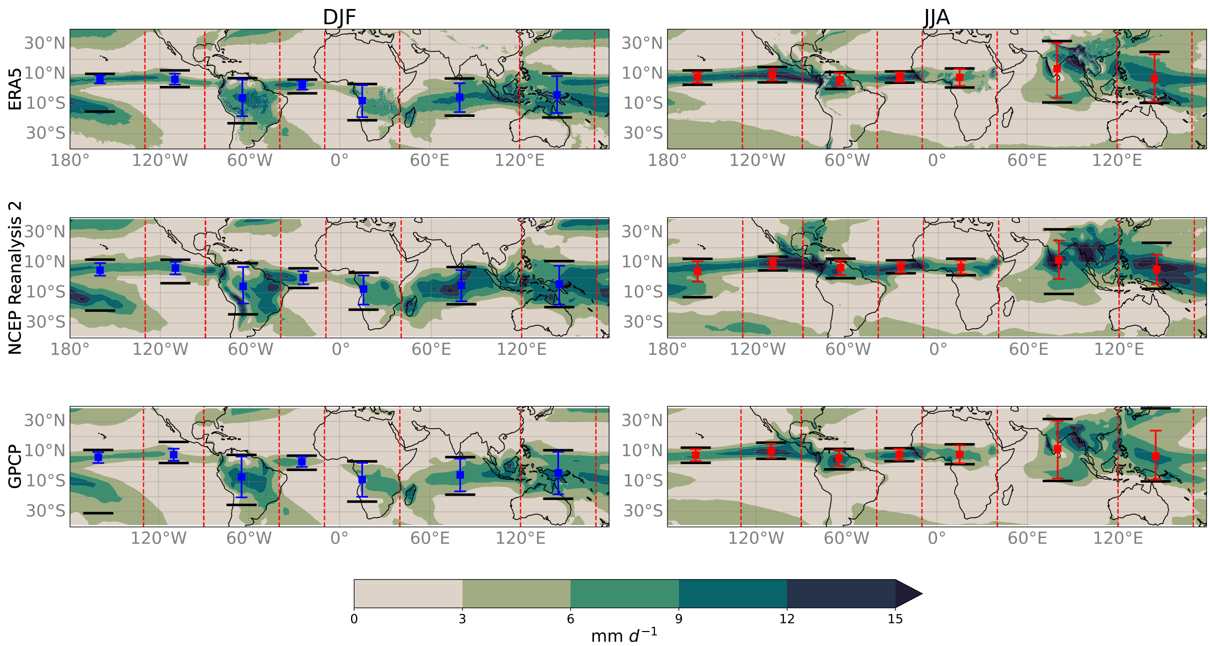

Figure A1. Seasonally averaged precipitation for the period 1980-2010 of ERA5, NCEP Reanalysis 2 and GPCP for DJF and JJA. The centre of the error bars indicates the median latitude of the ITCZ centre for each region, for the respective season over the years, while the caps show the median latitude for the edges of the ITCZ. The large black horizontal lines above and below the error bars show the 0.9 and 0.1 quantiles of latitudes of the northern and southern edges of the ITCZ, respectively.

Appendix A: Evaluation of Methodology

The ITCZ identification methodology of Sect. 3.1 was applied to seasonally averaged reanalysis (ERA5 and NCEP Reanalysis 2) and observational (GPCP) data for the years between 1980 and 2010 (Fig. A1).

The methodology identifies the location and edges of the ITCZ reasonably well for most cases. In the Central Pacific in DJF, the methodology generally correctly chooses the ITCZ for the majority of the years, since the median location of the ITCZ is confined over the ITCZ. For some of the years, though, the 0.1 quantile of the southern edge latitude is at or near the southern edge of the Southern Pacific Convergence Zone. This could be due to its large precipitation intensity, which can exceed that of the ITCZ in this part of the world, or due to the proximity of the two, which leads to the methodology identifying it as a single band.

During the JJA season, although the methodology generally identifies the ITCZ location across most regions, the northern edge extends into the mid-latitude storm track in certain areas, such as the Western Pacific. In the Indian Ocean region, where the ITCZ is less well defined and the monsoon dominates, the methodology identifies the monsoon rainbands as part of the ITCZ. This classification is a consequence of the precipitation-based detection method and should be interpreted accordingly.

https://doi.org/10.5194/egusphere-2026-5285
Preprint. Discussion started: 17 September 2026

By design, the methodology can be used with monthly averaged precipitation data, but also with seasonally and annually averaged data.

Appendix B: Evaluation of the models

The historical runs of the models were compared to the ERA5 reanalysis for the period 1981-2005. For OptimESM models, the corresponding CMIP6Plus historical runs were used. For the UKESM1-2-LL, there were 3 historical variants, for the EC-Earth3-ESM-1, 5 variants, for the IPSL-CM6-ESMCO2, 4 variants, and for the CNRM-ESM2-2, 1 variant. For the rest of the models, the CMIP6 (or the CMIP5 for the GFDL-ESM2M) historical runs were used. For the GFDL-ESM2M, 1 historical run was used, and for the MIROC-ES2L and NorESM2-LM 3 historical runs each.

Figure B1a,b indicates that most models exhibit significant precipitation biases in the equatorial regions of the major oceanic bodies during both seasons. Specifically, all models indicate a dipole of precipitation biases over the equatorial regions of the Atlantic for the DJF season, with positive biases at the south. All models have positive precipitation biases over most of the maritime continent (South-East Asia) for DJF. Additionally, all models except MIROC-ES2L have positive precipitation biases in the western equatorial part of the Indian Ocean, just east of Africa.

For the JJA season, all models have positive precipitation biases over the equatorial Atlantic region, with EC-Earth3-ESM-1 and UKESM1-2-LL models exhibiting notable negative precipitation biases just north of it. Most models except the UKESM1-2-LL have negative precipitation biases over the Western Pacific region. All models except MIROC-ES2L have negative precipitation biases in the equatorial Central and Eastern Pacific region, with positive biases just north and south of it.

Comparison of years 10–50 of the ramp-up TIPMIP simulations with the historical simulations for each model (Fig. B1c,d), corresponding to similar levels of warming ($\sim 0.2 - 1.0\ ^o$ C), shows only minor differences in precipitation for the majority of models. The largest differences are observed in the GFDL-ESM2M model, with increased precipitation in the ramp-up over the Western Pacific for both seasons, and decreased precipitation over the Central Pacific in DJF. In the NorESM2-LM, there is a small but notable precipitation difference dipole, with positive values just north of the equator and negative just south of the equator, over most of the equatorial regions of the planet, for both seasons. A similar, but weaker, precipitation difference dipole is observed in the UKESM1-2-LL model, but only in the DJF season.

The small precipitation differences between the early years of the ramp-up simulations and the historical runs at comparable warming levels lends confidence to the use of the zero-emission protocol, initialized from the ramp-up simulations at specified GWLs, and suggest that it produces realistic precipitation changes at those warming levels.

Utilizing the MSPAEF metric (Karpasitis et al., 2026) to quantify the general performance of the models more precisely (Fig. B2), it is evident that the EC-Earth3-ESM-1 model performs the best at representing the precipitation distribution out of the models used in this study, for most seasons, but not for the annually averaged precipitation, where UKESM1-2-LL and NorESM2-LM perform better than it. On the other hand, the GFDL-ESM2M has the worst performance in the representation of precipitation, which is expected since it is an earlier generation model than the rest, as the only CMIP5 model of the

https://doi.org/10.5194/egusphere-2026-5285
Preprint. Discussion started: 17 September 2026

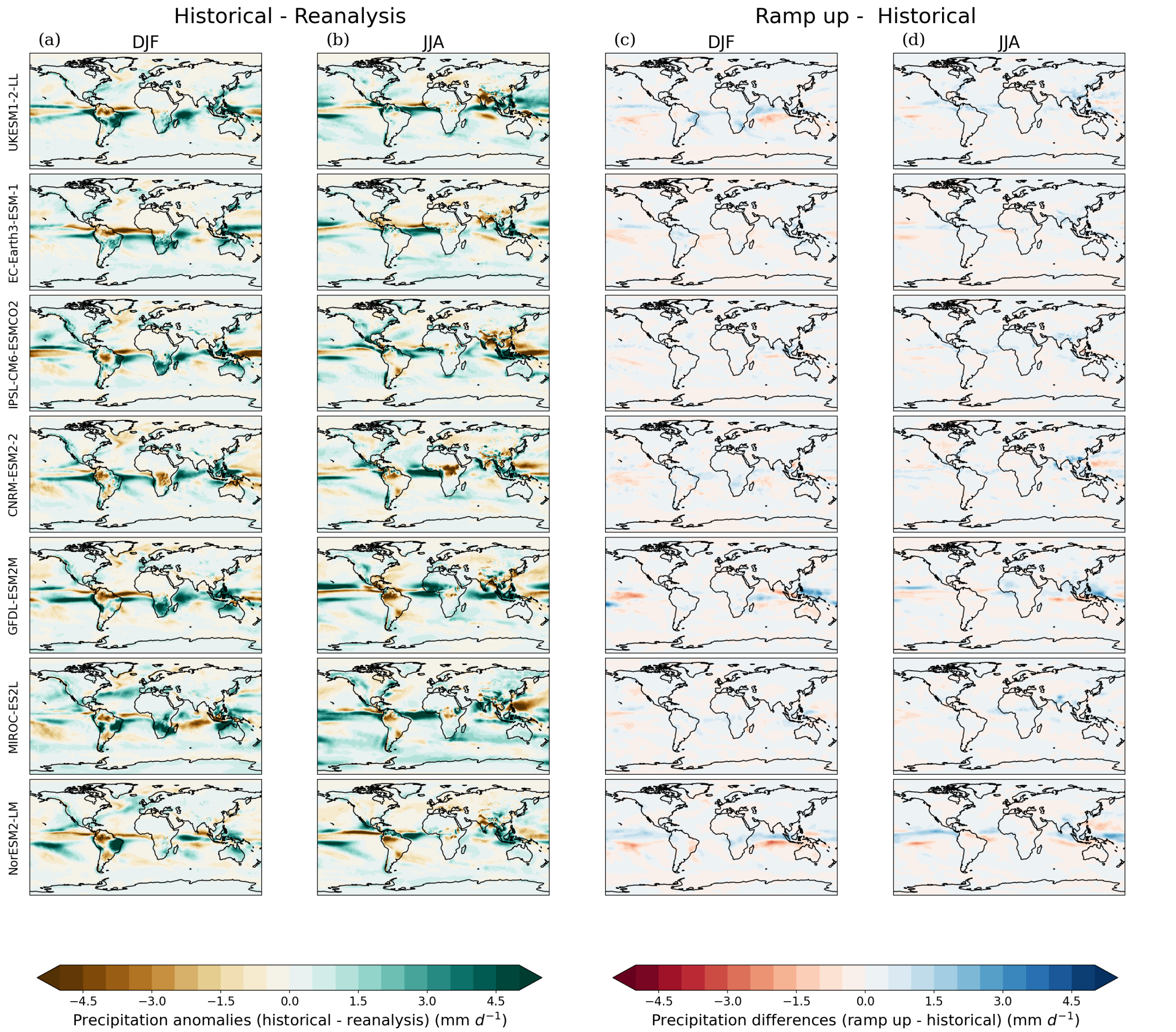

Figure B1. Historical precipitation evaluation and precipitation differences of TIPMIP ramp-up experiments compared to historical runs for each model. Columns (a) and (b) display model precipitation anomalies relative to ERA5 reanalysis for the historical reference period (1981–2005) during the DJF and JJA seasons, respectively. Columns (c) and (d) show the precipitation differences between the initial phase of the TIPMIP ramp-up simulations (years 10–50) and the historical baseline period (1981–2005) for the DJF and JJA seasons, respectively.

https://doi.org/10.5194/egusphere-2026-5285
Preprint. Discussion started: 17 September 2026

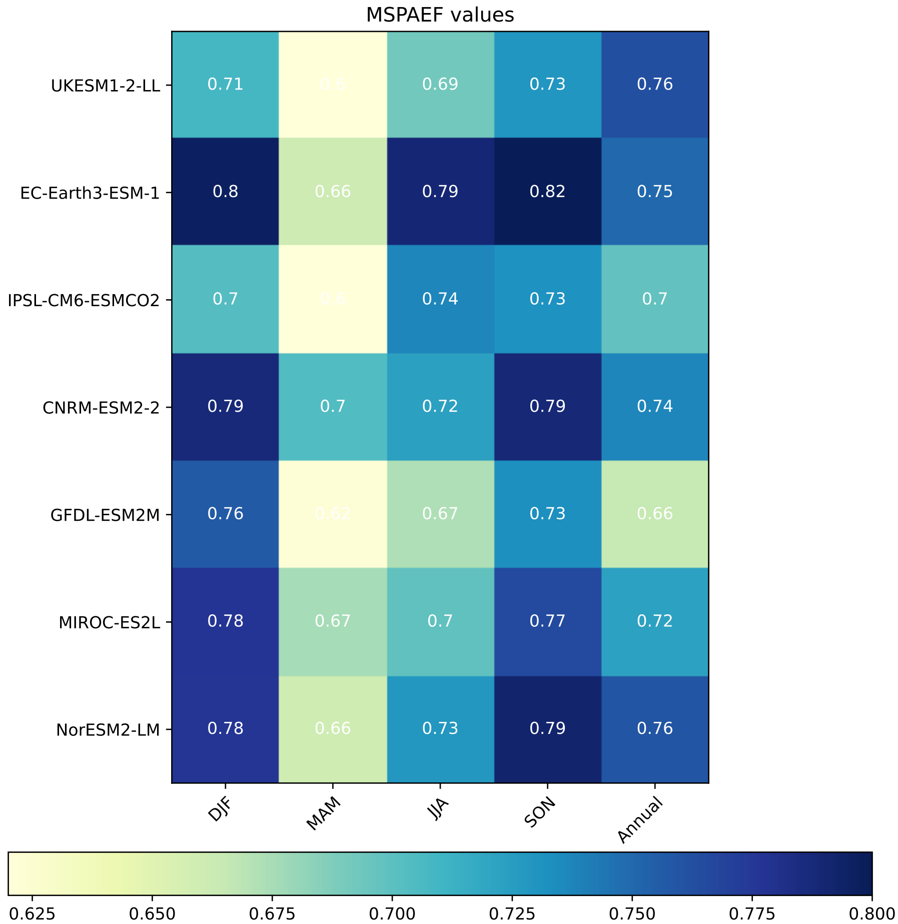

Figure B2. Heatmap of MSPAEF metric values for the historical runs of the TIPMIP models compared to the ERA5 reanalysis of the tropical precipitation (20^o S to 20^o N) for the different seasons of the period 1981-2005.

ensemble. Generally, all models have better performance at representing precipitation during the DJF and SON seasons, while they struggle more in the MAM and JJA seasons.

To further assess model performance in representing the ITCZ, we employ the Tropical Precipitation Asymmetry Index (TPAI) and the Equatorial Precipitation Index (EPI) (Tian and Dong, 2020) in the Pacific region (120^o E to 80^o W), which provide quantitative measures of the double ITCZ bias. Higher values of both indices indicate a reduced double ITCZ bias and, therefore, a more realistic simulation of tropical precipitation.

As shown in Fig. B3, most models (except MIROC-ES2L) exhibit lower Pacific TPAI and EPI values compared to the reanalysis and observational datasets, indicating a pronounced double ITCZ bias across most of the ensemble. Among the models, IPSL-CM6-ESMCO2 stands out with particularly low EPI values, suggesting an overly strong equatorial cold tongue and suppressed precipitation along the equator. In contrast, NorESM2-LM shows the worst performance in the TPAI index,

https://doi.org/10.5194/egusphere-2026-5285
Preprint. Discussion started: 17 September 2026

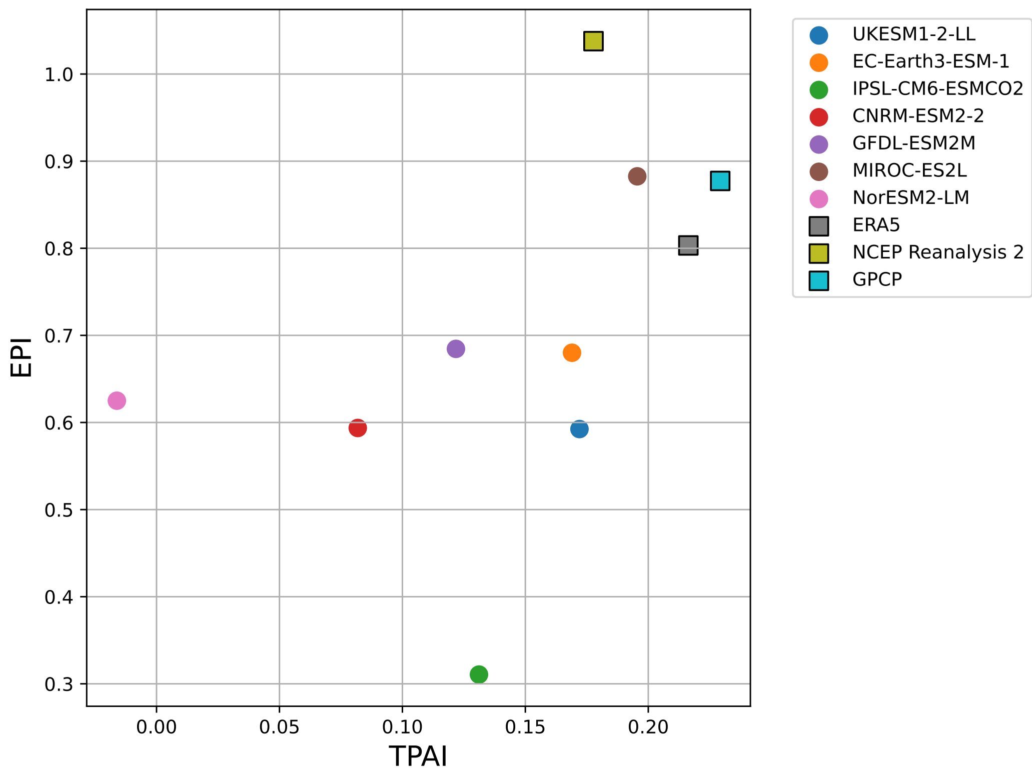

Figure B3. Scatter plot of Pacific TPAI versus EPI double ITCZ indices for the 1981–2005 period. Each point represents the mean value from the historical simulations of the TIPMIP models, averaged across available ensemble members. Observational and reanalysis estimates from ERA5, NCEP Reanalysis 2, and GPCP are shown for comparison. Circles denote model results, while squares indicate observational and reanalysis datasets.

indicating increased precipitation in the southern part of the equatorial Pacific, which is also evident in Fig. B1. The MIROC-ES2L is the only models whose EPI and TPAI values are really close to the reanalysis and observations, indicating it has the least double ITCZ bias of the models.

Code and data availability. The Python code used in this work can be obtained from https://doi.org/10.5281/zenodo.21787106 (Karpasitis, 2026a). The ERA5 data are publicly available from the Copernicus Climate Data Store (CDS) at https://cds.climate.copernicus.eu/datasets/reanalysis-era5-single-levels-monthly-means (ECMWF, 2019). The GPCP data are available at https://www.ncei.noaa.gov/access/metadata/landing-page/bin/iso?id=gov.noaa.ncdc:C00979 (NCEI, 2022). The NCEP Reanalysis 2 data are publicly available at https://psl.noaa.gov/data/gridded/data.ncep.reanalysis2.html (NCEP, 2022). The original TIPMIP model output datasets are not yet publicly available and are expected to be released through the official TIPMIP data archive. Due to their large size, the complete model output cannot be included with

https://doi.org/10.5194/egusphere-2026-5285
Preprint. Discussion started: 17 September 2026

this publication. To facilitate reproducibility, reduced processed datasets containing the intermediate analysis fields used for figure generation are provided through the Zenodo repository associated with this study at https://doi.org/10.5281/zenodo.21818785 (Karpasitis, 2026b).

Author contributions. AK and GZ designed the methodology. AK performed calculations and led manuscript writing; GZ, PH, IB, CJ and KW reviewed the paper. MA, IB, FF, TF, CJ, RS, TT, JW, KW, and TY provided the data.

Competing interests. The authors declare that they have no conflict of interest

Acknowledgements. This study was supported by the OptimESM project that has received funding from the European Union's Horizon Europe research and innovation programme under grant agreement No101081193. CJ acknowledges funding from the Horizon Europe project OptimESM "Optimal High Resolution Earth System Models for Exploring Future Climate Changes" (grant agreement no. 101081193); TipESM "Exploring Tipping Points and Their Impacts Using Earth System Models" funded by the European Union (grant agreement no. 101137673) and the associated the UK government's Horizon Europe funding guarantee (grant numbers, 10103098, 10043072)

https://doi.org/10.5194/egusphere-2026-5285
Preprint. Discussion started: 17 September 2026

References

Adam, O., Bischoff, T., and Schneider, T.: Seasonal and interannual variations of the energy flux equator and ITCZ. Part I: Zonally averaged ITCZ position, Journal of Climate, 29, 3219–3230, https://doi.org/10.1175/JCLI-D-15-0512.1, 2016a.

Adam, O., Bischoff, T., and Schneider, T.: Seasonal and interannual variations of the energy flux equator and ITCZ. Part II: Zonally varying shifts of the ITCZ, Journal of Climate, 29, 7281–7293, https://doi.org/10.1175/JCLI-D-15-0710.1, 2016b.

Adler, R. F., Sapiano, M. R., Huffman, G. J., Wang, J. J., Gu, G., Bolvin, D., Chiu, L., Schneider, U., Becker, A., Nelkin, E., Xie, P., Ferraro, R., and Shin, D. B.: The Global Precipitation Climatology Project (GPCP) monthly analysis (New Version 2.3) and a review of 2017 global precipitation, Atmosphere, 9, https://doi.org/10.3390/atmos9040138, 2018.

Berry, G. and Reeder, M. J.: Objective identification of the intertropical convergence Zone: Climatology and trends from the ERA-Interim, Journal of Climate, 27, 1894–1909, https://doi.org/10.1175/JCLI-D-13-00339.1, 2014.

Bischoff, T. and Schneider, T.: Energetic constraints on the position of the intertropical convergence zone, Journal of Climate, 27, 4937–4951, https://doi.org/10.1175/jcli-d-13-00650.1, 2014.

Bossert, I., Baur, S., Cussac, M., Berthet, S., Delire, C., Michou, M., Nabat, P., Roehrig, R., Voldoire, A., and Séférian, R.: CNRM-ESM2-2: development and evaluation of an updated version of the CNRM-CERFACS Earth System Model, ESS Open Archive, https://doi.org/10.22541/essoar.175977424.42948487/v1, 2025.

Boucher, O., Servonnat, J., Albright, A. L., Aumont, O., Balkanski, Y., Bastrikov, V., Bekki, S., Bonnet, R., Bony, S., Bopp, L., Braconnot, P., Brockmann, P., Cadule, P., Caubel, A., Cheruy, F., Codron, F., Cozic, A., Cugnet, D., D'Andrea, F., Davini, P., de Lavergne, C., Denvil, S., Deshayes, J., Devilliers, M., Ducharne, A., Dufresne, J. L., Dupont, E., Éthé, C., Fairhead, L., Falletti, L., Flavoni, S., Foujols, M. A., Gardoll, S., Gastineau, G., Ghattas, J., Grandpeix, J. Y., Guenet, B., Lionel, E. G., Guilyardi, E., Guimberteau, M., Hauglustaine, D., Hourdin, F., Idelkadi, A., Joussaume, S., Kageyama, M., Khodri, M., Krinner, G., Lebas, N., Levavasseur, G., Lévy, C., Li, L., Lott, F., Lurton, T., Luyssaert, S., Madec, G., Madeleine, J. B., Maignan, F., Marchand, M., Marti, O., Mellul, L., Meurdesoif, Y., Mignot, J., Musat, I., Ottlé, C., Peylin, P., Planton, Y., Polcher, J., Rio, C., Rochetin, N., Rousset, C., Sepulchre, P., Sima, A., Swingedouw, D., Thiéblemont, R., Traore, A. K., Vancoppenolle, M., Vial, J., Vialard, J., Viovy, N., and Vuichard, N.: Presentation and Evaluation of the IPSL-CM6A-LR Climate Model, Journal of Advances in Modeling Earth Systems, 12, https://doi.org/10.1029/2019MS002010, 2020.

Brown, J. R., Lengaigne, M., Lintner, B. R., Widlansky, M. J., van der Wiel, K., Dutheil, C., Linsley, B. K., Matthews, A. J., and Renwick, J.: South Pacific Convergence Zone dynamics, variability and impacts in a changing climate, https://doi.org/10.1038/s43017-020-0078-2, 2020.

Byrne, M. P. and Schneider, T.: Energetic constraints on the width of the intertropical convergence zone, Journal of Climate, 29, 4709–4721, https://doi.org/10.1175/JCLI-D-15-0767.1, 2016a.

Byrne, M. P. and Schneider, T.: Narrowing of the ITCZ in a warming climate: Physical mechanisms, Geophysical Research Letters, 43, 11,350–11,357, https://doi.org/10.1002/2016GL070396, 2016b.

Byrne, M. P., Pendergrass, A. G., Rapp, A. D., and Wodzicki, K. R.: Response of the Intertropical Convergence Zone to Climate Change: Location, Width, and Strength, Current Climate Change Reports, 4, 355–370, https://doi.org/10.1007/s40641-018-0110-5, 2018.

Chopra, G., Unni, V. R., Venkatesan, P., Vallejo-Bernal, S. M., Marwan, N., Kurths, J., and Sujith, R. I.: Community structure of tropics emerging from spatio-temporal variations in the Intertropical Convergence Zone dynamics, Scientific reports, 14, 24 463, https://doi.org/10.1038/s41598-024-73872-0, 2024.

https://doi.org/10.5194/egusphere-2026-5285
Preprint. Discussion started: 17 September 2026

Dixit, V., Geoffroy, O., and Sherwood, S. C.: Control of ITCZ Width by Low-Level Radiative Heating From Upper-Level Clouds in Aquaplanet Simulations, Geophysical Research Letters, 45, 5788–5797, https://doi.org/10.1029/2018GL078292, 2018.

Donohoe, A., Marshall, J., Ferreira, D., and Mcgee, D.: The relationship between ITCZ location and cross-equatorial atmospheric heat transport: From the seasonal cycle to the last glacial maximum, Journal of Climate, 26, 3597–3618, https://doi.org/10.1175/JCLI-D-12-00467.1, 2013.

Dunne, J. P., John, J. G., Adcroft, A. J., Griffies, S. M., Hallberg, R. W., Shevliakova, E., Stouffer, R. J., Cooke, W., Dunne, K. A., Harrison, M. J., Krasting, J. P., Malyshev, S. L., Milly, P. C., Phillipps, P. J., Sentman, L. T., Samuels, B. L., Spelman, M. J., Winton, M., Wittenberg, A. T., and Zadeh, N.: GFDL's ESM2 global coupled climate-carbon earth system models. Part I: Physical formulation and baseline simulation characteristics, Journal of Climate, 25, 6646–6665, https://doi.org/10.1175/JCLI-D-11-00560.1, 2012.

Döscher, R., Acosta, M., Alessandri, A., Anthoni, P., Arsouze, T., Bergman, T., Bernardello, R., Boussetta, S., Caron, L. P., Carver, G., Castrillo, M., Catalano, F., Cvijanovic, I., Davini, P., Dekker, E., Doblas-Reyes, F. J., Docquier, D., Echevarria, P., Fladrich, U., Fuentes-Franco, R., Gröger, M., Hardenberg, J. V., Hieronymus, J., Karami, M. P., Keskinen, J. P., Koenigk, T., Makkonen, R., Massonnet, F., Ménégoz, M., Miller, P. A., Moreno-Chamarro, E., Nieradzik, L., Noije, T. V., Nolan, P., O'donnell, D., Ollinaho, P., Oord, G. V. D., Ortega, P., Prims, O. T., Ramos, A., Reerink, T., Rousset, C., Ruprich-Robert, Y., Sager, P. L., Schmith, T., Schrödner, R., Serva, F., Sicardi, V., Madsen, M. S., Smith, B., Tian, T., Tourigny, E., Uotila, P., Vancoppenolle, M., Wang, S., Wårlind, D., Willén, U., Wyser, K., Yang, S., Yepes-Arbós, X., and Zhang, Q.: The EC-Earth3 Earth system model for the Coupled Model Intercomparison Project 6, Geoscientific Model Development, 15, 2973–3020, https://doi.org/10.5194/gmd-15-2973-2022, 2022.

ECMWF: ECMWF ERA5 Reanalysis, https://cds.climate.copernicus.eu/datasets/reanalysis-era5-single-levels-monthly-means, 2019.

Frierson, D. M. and Hwang, Y. T.: Extratropical influence on ITCZ shifts in slab ocean simulations of global warming, Journal of Climate, 25, 720–733, https://doi.org/10.1175/JCLI-D-11-00116.1, 2012.

Frierson, D. M., Lu, J., and Chen, G.: Width of the Hadley cell in simple and comprehensive general circulation models, Geophysical Research Letters, 34, https://doi.org/10.1029/2007GL031115, 2007.

Green, B., Marshall, J., and Donohoe, A.: Twentieth century correlations between extratropical SST variability and ITCZ shifts, Geophysical Research Letters, 44, 9039–9047, https://doi.org/10.1002/2017GL075044, 2017.

Grise, K. M. and Davis, S. M.: Hadley cell expansion in CMIP6 models, Atmospheric Chemistry and Physics, 20, 5249–5268, https://doi.org/10.5194/acp-20-5249-2020, 2020.

Hajima, T., Watanabe, M., Yamamoto, A., Tatebe, H., Noguchi, M. A., Abe, M., Ohgaito, R., Ito, A., Yamazaki, D., Okajima, H., Ito, A., Takata, K., Ogochi, K., Watanabe, S., and Kawamiya, M.: Development of the MIROC-ES2L Earth system model and the evaluation of biogeochemical processes and feedbacks, Geoscientific Model Development, 13, https://doi.org/10.5194/gmd-13-2197-2020, 2020.

Hartmann, D. L.: Global physical climatology: Second Edition, Elsevier, https://doi.org/10.1016/C2009-0-00030-0, 2015.

Hawkins, E. and Sutton, R.: Time of emergence of climate signals, Geophysical Research Letters, 39, https://doi.org/10.1029/2011GL050087, 2012.

Held, I. M. and Soden, B. J.: Robust responses of the hydrological cycle to global warming, Journal of Climate, 19, https://doi.org/10.1175/JCLI3990.1, 2006.

Hersbach, H., Bell, B., Berrisford, P., Hirahara, S., Horányi, A., Muñoz-Sabater, J., Nicolas, J., Peubey, C., Radu, R., Schepers, D., Simmons, A., Soci, C., Abdalla, S., Abellan, X., Balsamo, G., Bechtold, P., Biavati, G., Bidlot, J., Bonavita, M., Chiara, G. D., Dahlgren, P., Dee, D., Diamantakis, M., Dragani, R., Flemming, J., Forbes, R., Fuentes, M., Geer, A., Haimberger, L., Healy, S., Hogan, R. J., Hólm, E., Janisková, M., Keeley, S., Laloyaux, P., Lopez, P., Lupu, C., Radnoti, G., de Rosnay, P., Rozum, I., Vamborg, F., Villaume, S., and Thépaut, J. N.: The ERA5 global reanalysis, Quarterly Journal of the Royal Meteorological Society, 146, https://doi.org/10.1002/qj.3803, 2020.

Hu, Y., Huang, H., and Zhou, C.: Widening and weakening of the Hadley circulation under global warming, https://doi.org/10.1016/j.scib.2018.04.020, 2018.

Jones, C., Bossert, I., Dennis, D. P., Jeffery, H. A., Jones, C. D., Koenigk, T., Loriani, S., Sanderson, B., Séférian, R., Wyser, K., Yang, S., Abe, M., Bathiany, S., Braconnot, P., Brovkin, V., Burger, F. A., Cadule, P., Castruccio, F. S., Danabasoglu, G., Dittus, A., Donges, J. F., Fröb, F., Frölicher, T. L., Georgievski, G., Guo, C., Hu, A., Lawrence, P., Lerner, P., Licón-Saláiz, J., Otto-Bliesner, B., Romanou, A., Shevliakova, E., Silvy, Y., Swingedouw, D., Tjiputra, J., Walton, J., Wiltshire, A., Winkelmann, R., Wood, R., Yokohata, T., and Ziehn, T.: The TIPMIP Earth system model experiment protocol: phase 1, Geoscientific Model Development, 19, 6941–6966, https://doi.org/10.5194/gmd-19-6941-2026, 2026.

Kanamitsu, M., Ebisuzaki, W., Woollen, J., Yang, S. K., Hnilo, J. J., Fiorino, M., and Potter, G. L.: NCEP-DOE AMIP-II reanalysis (R-2), Bulletin of the American Meteorological Society, 83, https://doi.org/10.1175/bams-83-11-1631, 2002.

Karpasitis, A.: Code for the TIPMIP MMA on ITCZ and General Circulation changes, https://doi.org/10.5281/zenodo.21787106, 2026a.

Karpasitis, A.: Reduced datasets for the TIPMIP MMA on ITCZ and General Circulation changes, https://doi.org/10.5281/zenodo.21818785, 2026b.

Karpasitis, A., Hadjinicolaou, P., and Zittis, G.: A new efficiency metric for the spatial evaluation and inter-comparison of climate and geoscientific model output, Geoscientific Model Development, 19, https://doi.org/10.5194/gmd-19-345-2026, 2026.

Kjellsson, J.: Weakening of the global atmospheric circulation with global warming, Climate Dynamics, 45, https://doi.org/10.1007/s00382-014-2337-8, 2015.

Li, Y., Du, M., Feng, J., Xu, F., and Song, W.: Relationships between the Hadley circulation and tropical sea surface temperature with different meridional structures simulated in CMIP6 models, Frontiers in Marine Science, 10, https://doi.org/10.3389/fmars.2023.1145509, 2023.

Li, Z., Liu, T., Huang, Y., Peng, J., and Ling, Y.: Evaluation of the CMIP6 Precipitation Simulations Over Global Land, Earth's Future, 10, https://doi.org/10.1029/2021EF002500, 2022.

Liu, C., Liao, X., Qiu, J., Yang, Y., Feng, X., Allan, R. P., Cao, N., Long, J., and Xu, J.: Observed variability of intertropical convergence zone over 1998-2018, Environmental Research Letters, 15, https://doi.org/10.1088/1748-9326/aba033, 2020.

Mahony, C. R. and Cannon, A. J.: Wetter summers can intensify departures from natural variability in a warming climate, Nature Communications, 9, https://doi.org/10.1038/s41467-018-03132-z, 2018.

Mischell, E. and Lee, J. E.: Observed Zonal Variations of the Relationship between ITCZ Position and Meridional Temperature Contrast, Climate, 10, https://doi.org/10.3390/cli10030030, 2022.

Mulcahy, J. P., Jones, C. G., Rumbold, S. T., Kuhlbrodt, T., Dittus, A. J., Blockley, E. W., Yool, A., Walton, J., Hardacre, C., Andrews, T., Bodas-Salcedo, A., Stringer, M., Mora, L. D., Harris, P., Hill, R., Kelley, D., Robertson, E., and Tang, Y.: UKESM1.1: development and evaluation of an updated configuration of the UK Earth System Model, Geoscientific Model Development, 16, https://doi.org/10.5194/gmd-16-1569-2023, 2023.

NCEI: Global Precipitation Climatology Project v2.3 (GPCP), https://www.ncei.noaa.gov/access/metadata/landing-page/bin/iso?id=gov.noaa.ncdc:C00979, 2022.

NCEP: NCEP-DOE Reanalysis 2, https://psl.noaa.gov/data/gridded/data.ncep.reanalysis2.html, 2022.

Nicholson, S. E.: The ITCZ and the seasonal cycle over equatorial Africa, Bulletin of the American Meteorological Society, 99, 337–348, https://doi.org/10.1175/BAMS-D-16-0287.1, 2018.

https://doi.org/10.5194/egusphere-2026-5285
Preprint. Discussion started: 17 September 2026

Rajendran, K., Kitoh, A., and Srinivasan, J.: Effect of SST variation on ITCZ in APE simulations, Journal of the Meteorological Society of Japan, 91, 195–215, https://doi.org/10.2151/jmsj.2013-A06, 2013.

Ramotubei, T. S., Landman, W. A., Mateyisi, M. J., Nangombe, S. S., and Beraki, A. F.: Response of the global ITCZ to ENSO and how the ITCZ determined from maximum precipitation compares with the surface tropical wind convergence, Environmental Development, 55, https://doi.org/10.1016/j.envdev.2025.101210, 2025.

Roldán-Gómez, P. J., González-Rouco, J. F., Melo-Aguilar, C., and Smerdon, J. E.: The Role of Internal Variability in ITCZ Changes Over the Last Millennium, Geophysical Research Letters, 49, https://doi.org/10.1029/2021GL096487, 2022.

Schneider, T.: The general circulation of the atmosphere, Annual Review of Earth and Planetary Sciences, 34, 655–688, https://doi.org/10.1146/annurev.earth.34.031405.125144, 2006.

Sellar, A. A., Jones, C. G., Mulcahy, J. P., Tang, Y., Yool, A., Wiltshire, A., O'Connor, F. M., Stringer, M., Hill, R., Palmieri, J., Woodward, S., de Mora, L., Kuhlbrodt, T., Rumbold, S. T., Kelley, D. I., Ellis, R., Johnson, C. E., Walton, J., Abraham, N. L., Andrews, M. B., Andrews, T., Archibald, A. T., Berthou, S., Burke, E., Blockley, E., Carslaw, K., Dalvi, M., Edwards, J., Folberth, G. A., Gedney, N., Griffiths, P. T., Harper, A. B., Hendry, M. A., Hewitt, A. J., Johnson, B., Jones, A., Jones, C. D., Keeble, J., Liddicoat, S., Morgenstern, O., Parker, R. J., Predoi, V., Robertson, E., Siahaan, A., Smith, R. S., Swaminathan, R., Woodhouse, M. T., Zeng, G., and Zerroukat, M.: UKESM1: Description and Evaluation of the U.K. Earth System Model, Journal of Advances in Modeling Earth Systems, 11, 4513–4558, https://doi.org/10.1029/2019MS001739, 2019.

Smith, R. S., Mathiot, P., Siahaan, A., Lee, V., Cornford, S. L., Gregory, J. M., Payne, A. J., Jenkins, A., Holland, P. R., Ridley, J. K., and Jones, C. G.: Coupling the U.K. Earth System Model to Dynamic Models of the Greenland and Antarctic Ice Sheets, Journal of Advances in Modeling Earth Systems, 13, https://doi.org/10.1029/2021MS002520, 2021.

Son, S. W., Kim, S. Y., and Min, S. K.: Widening of the Hadley Cell from Last Glacial Maximum to future climate, Journal of Climate, 31, 267–281, https://doi.org/10.1175/JCLI-D-17-0328.1, 2018.

Stachnik, J. P. and Schumacher, C.: A comparison of the Hadley circulation in modern reanalyses, Journal of Geophysical Research Atmospheres, 116, https://doi.org/10.1029/2011JD016677, 2011.

Su, H., Jiang, J. H., Zhai, C., Shen, T. J., Neelin, J. D., Stephens, G. L., and Yung, Y. L.: Weakening and strengthening structures in the Hadley Circulation change under global warming and implications for cloud response and climate sensitivity, Journal of Geophysical Research, 119, https://doi.org/10.1002/2014JD021642, 2014.

Tian, B. and Dong, X.: The Double-ITCZ Bias in CMIP3, CMIP5, and CMIP6 Models Based on Annual Mean Precipitation, Geophysical Research Letters, 47, https://doi.org/10.1029/2020GL087232, 2020.

Vecchi, G. A. and Soden, B. J.: Global warming and the weakening of the tropical circulation, Journal of Climate, 20, https://doi.org/10.1175/JCLI4258.1, 2007.

Villela, R. J.: The south Atlantic convergence zone: A critical view and overview, https://doi.org/10.5935/0100-929X.20170006, 2017.

Vincent, D. G.: The South Pacific convergence zone (SPCZ): a review, Monthly Weather Review, 122, https://doi.org/10.1175/1520-0493(1994)122<1949:TSPCZA>2.0.CO;2, 1994.

Waliser, D. E. and Gautier, C.: A satellite-derived climatology of the ITCZ, Journal of Climate, 6, https://doi.org/10.1175/1520-0442(1993)006<2162:ASDCOT>2.0.CO;2, 1993.

Waliser, D. E. and Somerville, R. C. J.: Preferred Latitudes of the Intertropical Convergence Zone, Journal of the Atmospheric Sciences, 51, https://doi.org/10.1175/1520-0469(1994)051<1619:plotic>2.0.co;2, 1994.

Watt-Meyer, O. and Frierson, D. M.: ITCZ width controls on Hadley cell extent and eddy-driven jet position and their response to warming, Journal of Climate, 32, 1151–1166, https://doi.org/10.1175/JCLI-D-18-0434.1, 2019.

Wei, H. H. and Bordoni, S.: Energetic Constraints on the Intertropical Convergence Zone Position in the Observed Seasonal Cycle From Modern-Era Retrospective Analysis for Research and Applications, Version 2 (MERRA-2), Geophysical Research Letters, 47, https://doi.org/10.1029/2020GL088506, 2020.

Winkelmann, R., Dennis, D. P., Donges, J. F., Loriani, S., Klose, A. K., Abrams, J. F., Alvarez-Solas, J., Albrecht, T., Armstrong McKay, D., Bathiany, S., Blasco Navarro, J., Brovkin, V., Burke, E., Danabasoglu, G., Donner, R. V., Drüke, M., Georgievski, G., Goelzer, H., Harper, A. B., Hegerl, G., Hirota, M., Hu, A., Jackson, L. C., Jones, C., Kim, H., Koenigk, T., Lawrence, P., Lenton, T. M., Liddy, H., Licón-Saláiz, J., Menthon, M., Montoya, M., Nitzbon, J., Nowicki, S., Otto-Bliesner, B., Pausata, F., Rahmstorf, S., Ramin, K., Robinson, A., Rockström, J., Romanou, A., Sakschewski, B., Schädel, C., Sherwood, S., Smith, R. S., Steinert, N. J., Swingedouw, D., Willeit, M., Weijer, W., Wood, R., Wyser, K., and Yang, S.: The Tipping Points Modelling Intercomparison Project (TIPMIP): Assessing tipping point risks in the Earth system, EGUsphere, 2025, 1–52, https://doi.org/10.5194/egusphere-2025-1899, 2025.

Wodzicki, K. R. and Rapp, A. D.: Long-term characterization of the Pacific ITCZ using TRMM, GPCP, and ERA-Interim, Journal of Geophysical Research, 121, 3153–3170, https://doi.org/10.1002/2015JD024458, 2016.

Yang, J., He, S., and Bao, Q.: Convective/Large-scale Rainfall Partitions of Tropical Heavy Precipitation in CMIP6 Atmospheric Models, https://doi.org/10.1007/s00376-021-0238-4, 2021.

Yuan, S., Chiang, H. W., Liu, G., Bijaksana, S., He, S., Jiang, X., Imran, A. M., Wicaksono, S. A., and Wang, X.: The strength, position, and width changes of the intertropical convergence zone since the Last Glacial Maximum, Proceedings of the National Academy of Sciences of the United States of America, 120, https://doi.org/10.1073/pnas.2217064120, 2023.

Yun, K. S., Timmermann, A., and Stuecker, M.: Synchronized spatial shifts of Hadley and Walker circulations, Earth System Dynamics, 12, 121–132, https://doi.org/10.5194/esd-12-121-2021, 2021.

Zhang, H., Ma, X., Zhao, S., and Kong, L.: Advances in Research on the ITCZ: Mean Position, Model Bias, and Anthropogenic Aerosol Influences, https://doi.org/10.1007/s13351-021-0203-2, 2021.

Zhou, W., Leung, L. R., Lu, J., Yang, D., and Song, F.: Contrasting Recent and Future ITCZ Changes From Distinct Tropical Warming Patterns, Geophysical Research Letters, 47, https://doi.org/10.1029/2020GL089846, 2020.

Øyvind Seland, Bentsen, M., Olivié, D., Toniazzo, T., Gjermundsen, A., Graff, L. S., Debernard, J. B., Gupta, A. K., He, Y. C., Kirkevåg, A., Schwinger, J., Tjiputra, J., Aas, K. S., Bethke, I., Fan, Y., Griesfeller, J., Grini, A., Guo, C., Ilicak, M., Karset, I. H. H., Landgren, O., Liakka, J., Moseid, K. O., Nummelin, A., Spensberger, C., Tang, H., Zhang, Z., Heinze, C., Iversen, T., and Schulz, M.: Overview of the Norwegian Earth System Model (NorESM2) and key climate response of CMIP6 DECK, historical, and scenario simulations, Geoscientific Model Development, 13, https://doi.org/10.5194/gmd-13-6165-2020, 2020.